의학박사 학위논문

대사성질환의 병태생리 및 약물 작용기전 이해를 위한 대사체학 연구: 청소년 비만과 메포민

Metabolomics for understanding of pathophysiology and drug action mechanism in metabolic diseases: adolescent obesity and metformin

2016 년 8 월

서울대학교 대학원

의과학과 의과학 전공

조 금 선

대사성질환의 병태생리 및 약물 작용기전 이해를 위한 대사체학 연구: 청소년 비만과 메포민

지도교수 유 경 상

이 논문을 의학박사 학위논문으로 제출함.

2016 년 8 월

서울대학교 대학원

의과학과 의과학 전공

조 금 선

조 금 선의 의학박사 학위논문을 인준함.

2016 년 8 월

위 원 장	박 종 완	(인)
부위원장	유 경 상	(인)
위 원	장 인 진	(인)
위 원	조 주 연	(인)
위 원	황 금 숙	(인)

Metabolomics for understanding of pathophysiology and drug action mechanism in metabolic diseases: adolescent obesity and metformin

by

Kumsun Cho, M.S.

A Thesis Submitted to the Department of Biomedical Science
in Partial Fulfillment of the Requirements for the Degree of
Doctor of Philosophy in Medical Sciences (Biomedical Sciences)
at the Seoul National University Graduate School, Seoul, Korea

August 2016

Approved by Doctoral Committee:

Professor	Jong-Wan Park	Chairman
Professor	Kyung-Sang Yu	Vice chairman
Professor	In-Jin Jang	
Professor	Joo-Youn Cho	
Professor	Geum-Sook Hwang	

Abstract

Metabolomics for understanding of pathophysiology and drug action mechanism in metabolic diseases: adolescent obesity and metformin

Kumsun Cho

Major in Biomedical Sciences

Department of Biomedical Sciences

Seoul National University Graduate School

Metabolomics is a high-throughput method for assessing the pathophysiological state and for identifying novel biomarkers to understand molecular mechanisms of the disease. It has allowed the large-scale, simultaneous analysis of huge numbers of metabolites in biofluids particularly of metabolic diseases such as obesity and diabetes. The aim of this study was to investigate biomarkers affected by obesity and underlying molecular mechanisms of the anti-diabetic drug.

For identifying urinary biomarkers to distinguish metabolomic characteristics between obesity and normal weight in adolescents, adolescent subjects were divided into non-obese (n = 91) and obese (n = 93) groups according to body mass

index. Untargeted and targeted metabolomic profiling of urine was performed using high-performance liquid chromatography (LC)-quadrupole time-of-flight mass spectrometry (MS), and LC- and flow injection analysis-MS/MS systems, respectively. For identifying the novel underlying molecular mechanisms related to anti-diabetic effect of metformin, fourteen healthy male subjects were orally administered metformin (1000 mg) once. First morning urine samples were taken before and after administration to obtain metabolomic data. We then further investigated the anti-diabetic mechanism of metformin *in vitro* and *in vivo*.

In adolescent obesity biomarker study, multivariate statistical analysis showed clear discrimination between the untargeted metabolomes of nonobese and obese groups. Seven endogenous metabolites were distinguished in the obese group, and inflammation-related metabolite markers showed strong predictive power for group classification. From targeted metabolomics, 45 metabolites mostly related to inflammation were significantly different in the obese group. In underlying mechanism study of metformin, the fluctuation of the metabolite cortisol indicated that the neuroendocrine system was involved in the anti-diabetic effect of metformin. And we found that metformin induced AMPK/liver X receptor α (LXRα) phosphorylation, followed by pro-opiomelanocortin (POMC) suppression in rats.

Significantly different metabolome signatures were identified between normal weight and obese adolescents and before and after metformin treatment groups. These metabolomic studies demonstrated that inflammation-driven insulin resistance, ammonia toxicity, and oxidative stress may represent crucial metabolomic signatures in obese adolescents, and the anti-hyperglycemic effect of metformin is attributed to reduced POMC/adrenocorticotropic hormone (ACTH)/cortisol levels following AMPK/LXRα phosphorylation in the pituitaries.

Key Words: metabolomics, biomarker, adolescent obesity, diabetes, metformin

Student Number: 2012-31163

Table of Contents

Page

List of Tables

List of Figures

List of Abbreviations

BMI, body mass index

SBP, systolic blood pressure

DBP, diastolic blood pressure

AST, aspartate aminotransferase

ALT, alanine transaminase

Chol, cholesterol

TG, triglycerides

HDL, high-density lipoprotein

LDL, low-density lipoprotein

SMs, sphingomyelins

HPLC, high-performance liquid chromatography

QToF MS, quadrupole time-of-flight mass spectrometry

PCA, principal component analysis

FIA-MS/MS, flow injection analysis tandem mass spectrometry

MRM, multiple reaction monitoring

ROC, receiver operating characteristic

PSA, propensity score analysis

AMPK, AMP-activated protein kinase

LXRα, liver X receptor α

POMC, pro-opiomelanocortin

ACTH, adrenocorticotropic hormone

BBB, blood-brain-barrier

HPA, hypothalamic-pituitary-adrenal

Introduction

Advanced analytical techniques and data processing tools have been developed to discover biomarkers of various diseases. Metabolomics in particular has allowed the large-scale, simultaneous analysis of huge numbers of metabolites in human biofluids or tissues [1]. Recently, metabolomics has progressed remarkably within the past decade and provided mechanistic insights by correlating biochemical changes with phenotypes. Metabolomics-driven approaches have demonstrated immense potential for increasing our understanding of disease status [2], gut microbiome-host variations [3], and toxicological mechanisms [4]. An untargeted metabolomics approach is especially comprehensive in scope and can measure as many metabolites as possible from biological samples simultaneously, without bias. This has great potential for revealing the underlying mechanism of pathophysiology or drug effects. Therefore, these 'metabolomic' studies are seen as a useful tool for the study of metabolic diseases (e.g., obesity and diabetes) to investigate systemic alterations in metabolism or mechanism of its therapeutic drugs (e.g., metformin).

The pervasiveness of adolescent obesity has increased worldwide over the last few decades [5]. Adolescent obesity causes metabolic disturbances, including insulin resistance, dyslipidemia, and hypertension, which could promote the development of cardiovascular disorders in youth and through adulthood [6,7]. Accordingly, adolescent obesity has become a huge health challenge. Obesity arises from complicated interactions between genetic and environmental influences, including food and lifestyle. The identification of associated biomarkers to predict and prevent the occurrence of obesity-associated health risks in youth and beyond is therefore necessary.

Obesity is associated with metabolic disturbances in the whole body. Because metabolomics can readily detect subtle changes in metabolic networks, the investigation of metabolite concentrations may provide predictive biomarkers relevant to metabolic disorders and new insights into the biological mechanisms of adolescent obesity. However, unlike adult obesity, few studies have examined obesity-related metabolomic changes in adolescents. Given the major public health concerns related to obesity, biomarker exploration for the prediction and prevention of adolescent obesity and its related metabolic disorders is required.

Metformin is frequently prescribed for type 2 diabetes and has many of advantages including it is weight neutral [8], and it does not affect the risk of cardiovascular disease [9] and hypoglycemia [10]. Metformin exerts its antihyperglycemic action primarily by inhibiting hepatic gluconeogenesis and by increasing the action of insulin in certain target organs, like muscle [11] and fat [12]. Additionally, metformin is progressively used in polycystic ovary syndrome (PCOS) and many studies suggest that metformin could affect pituitary gonadotropin-secreting cells [13]. However, the underlying mechanism by which metformin regulates blood glucose levels and/or affects pituitary remains unknown.

It is well known that the pleiotropic actions of metformin are associated with AMP-activated protein kinase (AMPK) [14]. The pituitary-mediated actions of metformin were also elucidated in PCOS and diabetes. In particular, Lucie Tosca et al. elucidated that metformin-induced AMPK activation could exert its action in pituitary cells [13]. It was also supported by recent studies that orally-dosed metformin rapidly crosses the blood-brain-barrier (BBB) and accumulates in the pituitary gland and hypothalamus of rats [15]. However, the anti-hyperglycemic mechanism of metformin, associated with the neuroendocrine system, is not fully understood.

In this study, we used untargeted metabolomics and investigated urinary endogenous metabolites affected by obesity in adolescents and metformin administration in healthy subjects.

Part I:

Combined untargeted and targeted metabolomic profiling reveals urinary biomarkers for discriminating obese from normal weight adolescents

Materials and Methods

Study population

We extracted 100 obese subjects (body mass index [BMI] ≥ 99th percentile from baseline or BMI ≥ 30 kg/m^2) from 2457 participants in a school-based cohort registry recorded by the Korea Centers for Disease Control and Prevention in 2012. Obesity degree was defined by BMI according to Korean national criteria [16]. As controls, we selected 100 nonobese (25th < BMI < 75th percentiles from baseline) adolescents randomly matched for sex, age, and region via propensity score analysis (PSA) [17]. All subjects were without chronic illness. Seven obese subjects and nine controls had missing data and samples and were excluded.

All subjects underwent blood pressure screening by oscillometry and baseline laboratory examination. The healthy upper limits for systolic blood pressure (SBP), diastolic blood pressure (DBP), aspartate aminotransferase (AST), alanine transaminase (ALT), and cholesterol (Chol) were defined as 130 mmHg, 80 mmHg, 40 U/L, 40 U/L, and 170 mg/dL, respectively. And there was no strict limitation on dietary style because of a school-based cohort registry. However, dietary intake was assessed using a self-administered questionnaire and estimated dietary records documented over 3 consecutive days.

All participants and their parents were interviewed at home or were invited to visit a mobile examination center, where they were examined. Twelve-hour fasting blood and morning urine samples were collected from all subjects after providing informed consent. The study was carried out in accordance with the Declaration of Helsinki and Korean Good Clinical Practice (KGCP) and was approved by the Institutional Review Board of Seoul Paik Hospital (IIT-2012-092), Seoul, Korea.

High-performance liquid chromatography (HPLC)-quadrupole time-of-flight (QToF) mass spectrometry (MS)-based data acquisition for untargeted metabolomic profiling

Sample preparation

Urine samples were stored at −80°C immediately after collection. Aliquots were thawed and diluted five times with water. All samples were mixed for 10 min and centrifuged at 18,341 × *g* for 20 min at 4°C.

Chromatographic and TOF-MS conditions

Each sample (5 μL) was loaded onto a column held at 40°C and eluted with 0.1% formic acid and 20 mM ammonium formate in water (solvent A) and 0.1% formic acid in methanol (solvent B) over 21 min. While maintaining a constant flow rate of 0.4 mL/min, the metabolites were eluted using the following gradient: 2–98% B from 0.1 to 13 min, and 98% B held constant for 2 min followed by a return to 2% B from 15.1 to 17 min.

Chromatographic separations of metabolites in urine were performed with a Zorbax SB-C18, 50 × 2.1 mm, 1.8 μm (Agilent Technologies, Santa Clara, CA, USA) analytical column using an Agilent 1200 series HPLC system (Agilent Technologies).

The eluent was introduced into the Agilent 6530 QToF MS. The instrument settings were as follows: nebulizer gas pressure, 30 psi; temperature, 325°C; drying gas, 11 μL/min; capillary voltage, 3.5 kV; capillary temperature, 300°C; fragmentor voltage, 170 V; and skimmer voltage, 65 V. Centroid data were acquired over an *m/z* range of 100–1,100 using an accumulation time of 0.25 s per spectrum. The mass accuracy and mass resolution were less than 5 parts per million

(ppm) and ~20,000, respectively. Overall procedure quality was monitored using repeated extracts of a pooled urine sample (data not shown).

Data processing

All raw data files were converted to the compound exchange file format using MassHunter DA reprocessor software B.04.00 (Agilent Technologies). Mass Profiler Professional (MPP) software B.12.01 (Agilent Technologies) was used for aligning data and converting each metabolite feature (*m/z* × intensity × time) into a matrix of detected peaks versus compound identification. Each sample was normalized to the median of the baseline and log2 transformed. Samples were then aligned according to retention time and corrected according to the baseline.

Multivariate data analysis

The intensity of each ion was normalized to the total ion count to generate a multivariate data matrix consisting of the retention time, *m/z* value, and normalized peak area, which was analyzed by the MPP software package. Following the above data processing procedures, the MPP software was also employed to perform principal component analysis (PCA) for both positive and negative electrospray ionization (ESI) datasets to evaluate sample clustering according to obesity and to identify ions (filter thresholds: fold change ≤ 0.5 or fold change ≥ 2, and $P < 0.05$).

Biomarker identification

The resulting metabolites were identified using the human metabolome database (HMDB), METLIN, and the MS/MS fragment pattern of pure analytical standards. Specific metabolite identities were confirmed by comparing their mass spectra and chromatographic retention times with those obtained using commercially available

reference standards. Finally, the metabolites were quantified by normalization to creatinine levels in urine.

MS/MS-based data acquisition for targeted metabolite profiling

Targeted metabolomics of urine samples was performed using the Biocrates AbsoluteIDQ p180 kit (BIOCRATES Life Science AG, Innsbruck, Austria). This validated assay allows for simultaneous detection and quantification of metabolites in urine samples in a high-throughput manner. The methods were performed as described [18]. The urine samples were prepared according to the manufacturer's instructions and analyzed using an API 4000 QTRAP (Applied Biosystems/MDS Sciex, Foster City, CA, USA) operating in the multiple reaction monitoring (MRM) mode. The measurements were made in a 96-well format using the seven included calibration standards and three quality control samples. Briefly, flow injection analysis tandem mass spectrometry (FIA-MS/MS) was used to quantify a panel of 105 lipids simultaneously by MRM. Other metabolites were quantified using LC-MS/MS (scheduled MRM). A total of 186 metabolites or metabolite species were quantified including 40 acylcarnitines, 21 amino acids, 19 biogenic amines, 90 glycerophospholipids, 15 sphingolipids, and hexose. Data analysis was performed using MetIDQ software (BIOCRATES Life Science AG, Innsbruck, Austria). The abundance was calculated from the area under the curve by normalizing to the respective isotope-labeled internal standard. Phosphate-buffered saline (PBS) samples spiked with standard metabolites were used as quality controls to assess assay reproducibility.

Clustering analysis

Metabolite expression ratios of obese to nonobese adolescents (column) were log2 transformed and normalized using z-scores. In the vertical heatmap, color coding

indicated concentration differences for each metabolite (row): z-scores > 0 (red), < 0 (green), and ≈ 0 (black).

Chemicals

All chemicals were HPLC grade. Water and methanol were obtained from JT Baker (Phillipsburg, NJ, USA) and formic acid was purchased from Sigma-Aldrich (St. Louis, MO, USA).

Statistical analysis

We performed a PSA to select appropriate nonobese subjects without selection bias by excluding confounders [17]. PSA is a standard causal inference analysis recommended by the Patient Centered Outcomes Research Institute's Methodology Committee for comparative research using observational studies.

All data were analyzed using IBM SPSS Statistics 21 (Chicago, IL, USA), and the results were expressed as means and standard deviations. Data were statistically analyzed using the Student's t-test. Differences with *P* values of less than 0.05 were considered significant in two-tailed tests. The classification performance of the selected metabolites was assessed using the area under the receiver operating characteristic (ROC) curve (AUC).

Results

Baseline characteristics

In total, 184 adolescent obesity control/case samples were available for analysis. Despite matching for age and sex, significant differences in BMI, weight, waist circumference, hip circumference, SBP, DBP, AST, ALT, Chol, triglycerides (TG), high-density lipoprotein (HDL), and low-density lipoprotein (LDL) were identified (Table 1). Additionally, the dietary style of the obese and normal weight adolescents was compared, and we found that obese female adolescents consumed 16%, 15%, and 10% fewer calories than normal weight male and female adolescents and obese male adolescents, respectively (Fig. 1).

Untargeted metabolomic study of adolescent obesity

We performed untargeted metabolome analyses using HPLC-QToF MS to identify differently expressed metabolites between nonobese and obese adolescents. Frozen urine samples were thawed followed by large-scale metabolomics combined with multivariate data analyses. PCA showed significantly different metabolome signatures between groups (Fig. 2A).

We identified seven metabolites distinguishing metabolomic characteristics: 4-hydroxybenzaldehyde, hippuric acid, 4-sulfobenzyl alcohol, N,N-dimethyl-safingol, docosanoic acid, 4α-hydroxymethyl-5α-cholesta-8-en-3β-ol, and 12-oxo-20-carboxy-leukotriene B4 (Table 2 and Fig. 3). Additionally, we evaluated whether these differences were influenced by sex. Our results showed that levels of 4-sulfobenzyl alcohol and 4α-hydroxymethyl-5α-cholesta-8-en-3β-ol were decreased in female adolescents (Fig. 4).

ROC results for untargeted metabolomics

Untargeted metabolomic analysis revealed that metabolites related to inflammation or the microbiome to be discriminatory between nonobese and obese adolescents. ROC analysis to assess biomarker performance for group classification revealed inflammation-related metabolites (docosanoic acid, 12-oxo-20-carboxy-leukotriene B4, and 4α-hydroxymethyl-5α-cholesta-8-en-3β-ol) to be potent discriminators (Fig. 2B–2E and Table 3). These were highly correlated with several clinical parameters (BMI, AST, ALT, and Chol) closely associated with obesity complications, such as cardiovascular disease, liver disease, and metabolic syndrome. Therefore, further analysis by targeting metabolites related to metabolic diseases and inflammation was performed to identify the metabolomic patterns of obese adolescents.

Targeted metabolomic study of adolescent obesity

We next targeted and quantified metabolites belonging to lipid, amino acid, or biogenic amine classes using the AbsoluteIDQ p180 kit through combined LC-MS/MS and FIA-MS/MS. The constituent metabolites of the kit represent known markers related to various inflammatory or endocrine disorder phenotypes: e.g., oxidative stress, membrane composition and damage, energy metabolism, dyslipidemia, and insulin sensitivity/resistance. The mean values of the targeted metabolites between groups were tested using independent samples t-tests. We found that 45 metabolites were differentially expressed ($P < 0.05$) in urine, including nine acylcarnitines (carnitine, hydroxytetradecenoylcarnitine, propionylcarnitine, hydroxyvalerylcarnitine, hydroxypropionylcarnitine, butyrylcarnitine, hexenoylcarnitine, octanoylcarnitine, and nonaylcarnitine), 11 amino acids (arginine, asparagine, aspartate, glutamine, glycine, histidine, isoleucine, methionine, ornithine, serine, and threonine), seven biogenic amines

(asymmetric dimethylarginine, carnosine, 3,4-dihydroxyphenylalanine, dopamine, putrescine, serotonin, and total dimethylarginine), 14 glycerophospholipids (lysoPC a C18:0, PC aa C28:1, PC aa C30:2, PC aa C34:1, PC aa C34:2, PC aa C34:4, PC aa C36:1, PC aa C38:0, PC aa C38:6, PC aa C40:6, PC ae C38:5, PC ae C38:6, PC ae C44:4, and PC ae C44:5), and four sphingolipids (SM (OH) C14:1, SM (OH) C22:1, SM C16:0, and SM C24:1), as detailed in Table 4. We used a heatmap to visualize metabolomic signature differences and a supervised hierarchical clustering algorithm to uncover unknown metabolomic expression trends between groups (Fig. 5).

Table 1. Characteristics of phenotypic groups.

Parameter	Non-obese (N)	Obese (O)	*P*-value
N (n)	91	93	0.906
Sex (n, male / female)	47 / 44	53 / 40	-
Age (years)	13.83 ± 0.43	13.84 ± 0.52	0.906
BMI (percentile from baseline)	25^{th} - 75^{th}	≥ 99^{th} (or ≥ 30 kg/m^2)	-
Calculated BMI (kg/m^2)	20.52 ± 1.01	34.26 ± 2.88	< 0.001
Height (cm)	162.79 ± 6.47	164.64 ± 7.34	0.071
Weight (kg)	54.45 ± 5.00	93.30 ± 13.30	< 0.001
Waist circumference (cm)	70.01 ± 4.35	103.68 ± 8.25	< 0.001
Hip circumference (cm)	90.84 ± 3.33	113.16 ± 6.15	< 0.001
SBP (mm Hg)	112.86 ± 11.28	125.38 ± 13.34	< 0.001
DBP (mm Hg)	72.75 ± 7.76	79.03 ± 8.76	< 0.001
Glucose (mg/dL)	93.61 ± 7.44	93.29 ± 7.58	0.773
AST (U/L)	18.70 ± 3.48	29.38 ± 18.93	< 0.001
ALT (U/L)	11.84 ± 3.34	41.58 ± 39.71	< 0.001
Chol (mg/dl)	158.83 ± 29.08	179.08 ± 28.03	< 0.001
TG (mg/dl)	69.43 ± 41.34	127.86 ± 64.19	< 0.001
HDL (mg/dl)	54.75 ± 9.21	45.58 ± 7.96	< 0.001
LDL (mg/dL)	90.19 ± 25.04	107.92 ± 25.54	< 0.001

Data are presented as mean ± SD.

Table 2. Metabolites distinguishing metabolomic phenotype between non-obese and obese adolescents from untargeted analysis.

Metabolites	Non-obese ($\mu g/mg_{cre}$, n = 91)	Obese ($\mu g/mg_{cre}$, n = 93)	Mean FC (O/N)	*P*-value
4-Hydroxybenzaldehyde	18.32 ± 2.68	7.24 ± 1.41	0.40	< 0.001
Hippuric acid	409.89 ± 36.40	203.43 ± 20.56	0.50	< 0.001
4-Sulfobenzyl alcohol	8.88 ± 1.10	4.21 ± 0.36	0.47	< 0.001
N,N-dimethyl-Safingol	204.64 ± 8.24	97.41 ± 3.29	0.48	< 0.001
Docosanoic acid	70.12 ± 2.75	185.75 ± 6.87	2.65	< 0.001
4α-Hydroxymethyl-5α-cholesta-8-en-3β-ol	7.80 ± 0.83	23.04 ± 2.32	2.96	< 0.001
12-Oxo-20-carboxy-leukotriene B4	13.42 ± 0.55	31.00 ± 1.06	2.31	< 0.001

Data are presented as mean ± SE.

Table 3. ROC results for the untargeted metabolomics. Simple logistic models using metabolites identified from untargeted metabolomics were developed.

Metabolites (AUC, 95% CI)	4-Hydroxybenzaldehyde	Hippuric acid	4-Sulfobenzyl alcohol	N,N-dimethyl-Safingol	Docosanoic acid	4α-Hydroxymethyl-5α-cholesta-8-en-3β-ol	12-Oxo-20-carboxy-leukotriene B4
BMI	0.692, 0.62 - 0.77	0.757, 0.69 - 0.83	0.651, 0.57 - 0.73	0.956, 0.93 - 0.98	0.976, 0.96 - 0.99	0.824, 0.76 - 0.88	0.947, 0.92 - 0.98
SBP	0.642, 0.56 - 0.73	0.661, 0.58 - 0.74	0.505, 0.42 - 0.60	0.697, 0.65 - 0.80	0.728, 0.65 - 0.81	0.732, 0.66 - 0.81	0.725, 0.65 - 0.80
DBP	0.577, 0.49 - 0.66	0.598, 0.52 - 0.68	0.519, 0.44 - 0.60	0.601, 0.52 - 0.68	0.583, 0.50 - 0.67	0.600, 0.52 - 0.68	0.599, 0.52 - 0.68
AST	0.615, 0.49 - 0.74	0.643, 0.50 - 0.79	0.613, 0.47 - 0.76	0.802, 0.72 - 0.89	0.745, 0.65 - 0.84	0.784, 0.69 - 0.87	0.730, 0.64 - 0.82
ALT	0.665, 0.57 - 0.76	0.644, 0.53 - 0.76	0.606, 0.50 - 0.72	0.733, 0.65 - 0.82	0.813, 0.74 - 0.88	0.760, 0.68 - 0.84	0.782, 0.71 - 0.85
Chol	0.587, 0.50 - 0.67	0.549, 0.47 - 0.63	0.515, 0.43 - 0.60	0.655, 0.58 - 0.74	0.633, 0.55 - 0.72	0.607, 0.53 - 0.69	0.651, 0.57 - 0.73

Table 4. Metabolites distinguishing metabolomic phenotype between non-obese and obese adolescents from targeted analysis.

Metabolites	Non-obese (n = 91)	Obese (n = 93)	Mean FC (O/N)	*P*-value
Acylcarnitine (pM/nM$_{cre}$)				
Carnitine	6926.20 ± 754.66	11183.81 ± 6864.25	1.61	0.001
Hydroxytetradecenoylcarnitine	2.89 ± 0.10	2.52 ± 0.08	0.87	0.004
Propionylcarnitine	86.75 ± 9.39	142.23 ± 13.71	1.64	0.001
Hydroxyvalerylcarnitine	143.75 ± 6.21	193.30 ± 6.69	1.34	< 0.001
Hydroxypropionylcarnitine	1.29 ± 0.10	2.43 ± 0.15	1.88	< 0.001
Butyrylcarnitine	702.56 ± 39.76	565.44 ± 32.46	0.80	0.008
Hexenoylcarnitine	13.38 ± 0.73	17.37 ± 1.01	1.30	0.002
Octanoylcarnitine	60.81 ± 2.32	69.63 ± 2.32	1.15	0.008
Nonaylcarnitine	225.05 ± 13.63	153.82 ± 7.30	0.68	< 0.001
Amino acids (nM/nM$_{cre}$)				
Arginine	4.64 ± 0.16	4.05 ± 0.18	0.87	0.017
Asparagine	10.20 ± 0.41	7.70 ± 0.32	0.75	< 0.001
Aspartate	8.57 ± 0.40	10.59 ± 0.69	1.24	0.012
Glutamine	42.5 ± 1.70	34.15 ± 1.42	0.80	< 0.001
Glycine	114.02 ± 7.77	91.83 ± 7.43	0.81	0.040
Histidine	74.80 ± 3.41	84.36 ± 3.44	1.13	0.050
Isoleucine	1.40 ± 0.05	1.24 ± 0.04	0.89	0.013
Methionine	0.81 ± 0.03	0.68 ± 0.04	0.84	0.008
Ornithine	0.73 ± 0.04	0.55 ± 0.03	0.75	< 0.001

Serine	45.20 ± 2.10	30.87 ± 1.41	0.68	< 0.001
Thereonine	14.83 ± 0.83	11.32 ± 0.69	0.76	0.001
Biogenic amines (nM/nM$_{cre}$)				
Asymmetric dimethylarginine	3.67 ± 0.09	5.38 ± 0.12	1.47	< 0.001
Carnosine	1.76 ± 0.32	0.73 ± 0.04	0.41	0.002
3,4-Dihydroxyphenylalanine	0.03 ± 0.001	0.04 ± 0.002	1.33	0.007
Dopamine	0.25 ± 0.01	0.21 ± 0.007	0.84	0.001
Putrescine	0.07 ± 0.01	0.11 ± 0.01	1.57	0.014
Serotonin	0.10 ± 0.003	0.08 ± 0.00	0.80	0.001
Total dimethylarginine	9.21 ± 0.19	10.52 ± 0.19	1.14	< 0.001
Glycerophospholipids (pM/nM$_{cre}$)				
lysoPC a C18:0	5.02 ± 0.24	6.07 ± 0.35	1.21	0.013
PC aa C28:1	3.75 ± 0.19	1.89 ± 0.08	0.50	< 0.001
PC aa C30:2	0.13 ± 0.01	0.07 ± 0.01	0.54	< 0.001
PC aa C34:1	4.00 ± 0.35	2.86 ± 0.18	0.72	0.004
PC aa C34:2	4.06 ± 0.71	2.57 ± 0.24	0.63	0.047
PC aa C34:4	0.66 ± 0.15	0.34 ± 0.02	0.52	0.036
PC aa C36:1	2.35 ± 0.13	1.75 ± 0.10	0.74	< 0.001
PC aa C38:0	0.89 ± 0.04	1.04 ± 0.06	1.17	0.024
PC aa C38:6	0.13 ± 0.15	0.78 ± 0.08	6.00	0.034
PC aa C40:6	5.80 ± 0.23	6.83 ± 0.41	1.18	0.032
PC ae C38:5	5.82 ± 0.61	3.40 ± 0.29	0.58	< 0.001
PC ae C38:6	4.26 ± 0.22	1.65 ± 0.08	0.39	< 0.001
PC ae C44:4	2.13 ± 0.10	2.58 ± 0.18	1.21	0.033
PC ae C44:5	1.77 ± 0.09	2.29 ± 0.14	1.29	0.002

Sphingolipids (pM/nM_{cre})				
SM (OH) C14:1	0.23 ± 0.03	0.36 ± 0.04	1.57	0.020
SM (OH) C22:1	3.00 ± 0.17	2.22 ± 0.11	0.74	< 0.001
SM C16:0	8.92 ± 0.59	6.94 ± 0.42	0.78	0.007
SM C24:1	4.11 ± 0.27	3.07 ± 0.19	0.75	0.002

Data are presented as mean ± SE.

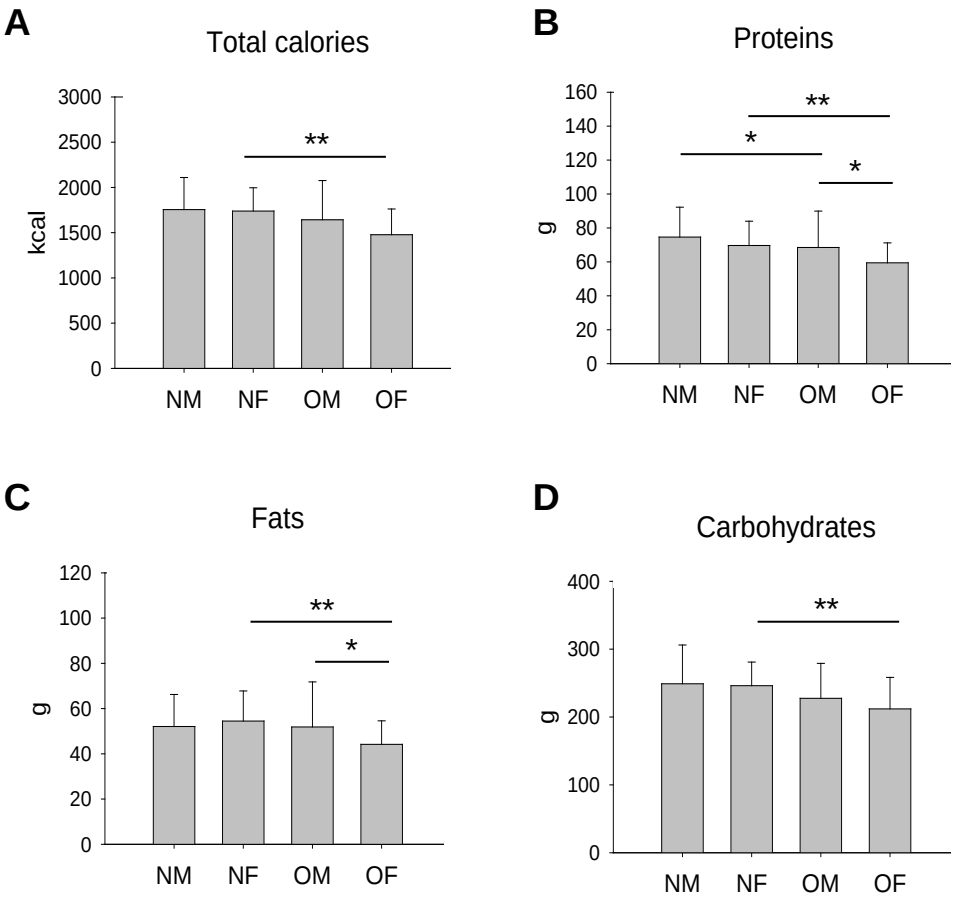
A
Total calories
kcal
3000
2500
2000
1500
1000
500
0
**
NM
NF
OM
OF
B
Proteins
g
160
140
120
100
80
60
40
20
0
**
*
*
NM
NF
OM
OF
C
Fats
g
120
100
80
60
40
20
0
**
*
NM
NF
OM
OF
D
Carbohydrates
g
400
300
200
100
0
**
NM
NF
OM
OF

* $P < 0.05$, ** $P < 0.01$

Figure 1. Bar graphs of the dietary style in the nonobese male (NM), nonobese female (NF), obese male (OM), and obese female (OF): (A) total calories, (B) proteins, (C) fats, and (D) carbohydrates.

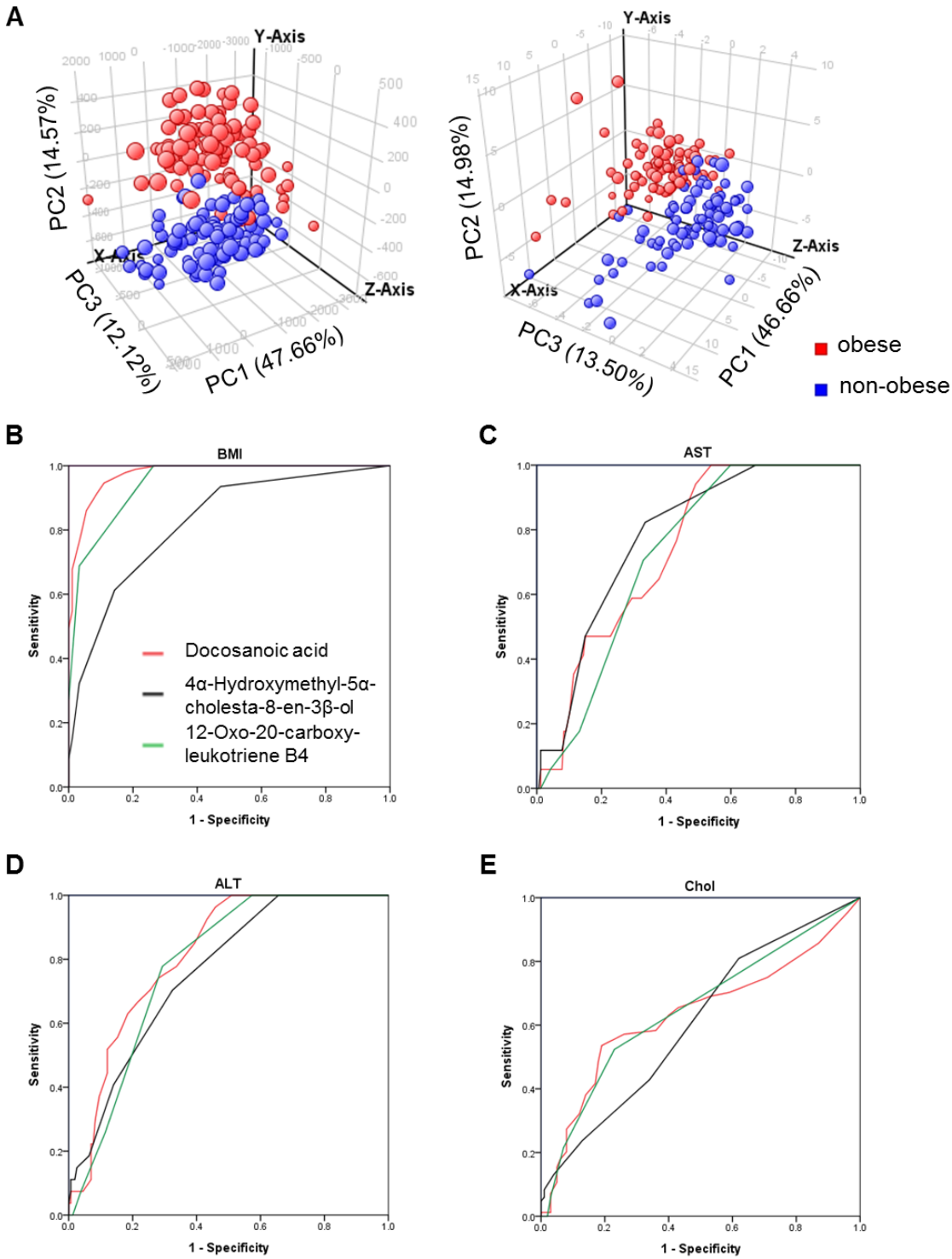
A
Y-Axis
PC2 (14.57%)
X-Axis
Z-Axis
PC3 (12.12%)
PC1 (47.66%)
Y-Axis
PC2 (14.98%)
Z-Axis
X-Axis
PC3 (13.50%)
PC1 (46.66%)
obese
non-obese
B
BMI
Sensitivity
1 - Specificity
Docosanoic acid
4α-Hydroxymethyl-5α-cholesta-8-en-3β-ol
12-Oxo-20-carboxy-leukotriene B4
C
AST
Sensitivity
1 - Specificity
D
ALT
Sensitivity
1 - Specificity
E
Chol
Sensitivity
1 - Specificity

Figure 2. Discovery of metabolite markers for obesity and its complications in adolescents. (A) Untargeted metabolomic profiling using HPLC-QToF MS generated PCA score plots discriminating the obese (*red*) from the nonobese adolescent group (*blue*). Data are shown for the positive (*left panel*) and negative (*right panel*) electrospray ionization (ESI) datasets. Plots of ROC results from the simple logistic models using docosanoic acid (*red*), 4α-hydroxymethyl-5α-cholesta-8-en-3β-ol (*black*), and 12-oxo-20-carboxy-leukotriene B4 (*green*) were generated and applied to determine the models of **(B)** BMI, **(C)** AST, **(D)** ALT, and **(E)** Chol for classifying the nonobese and obese groups. The ROC plots represent sensitivity (true positive rate) versus 1 − specificity (false positive rate).

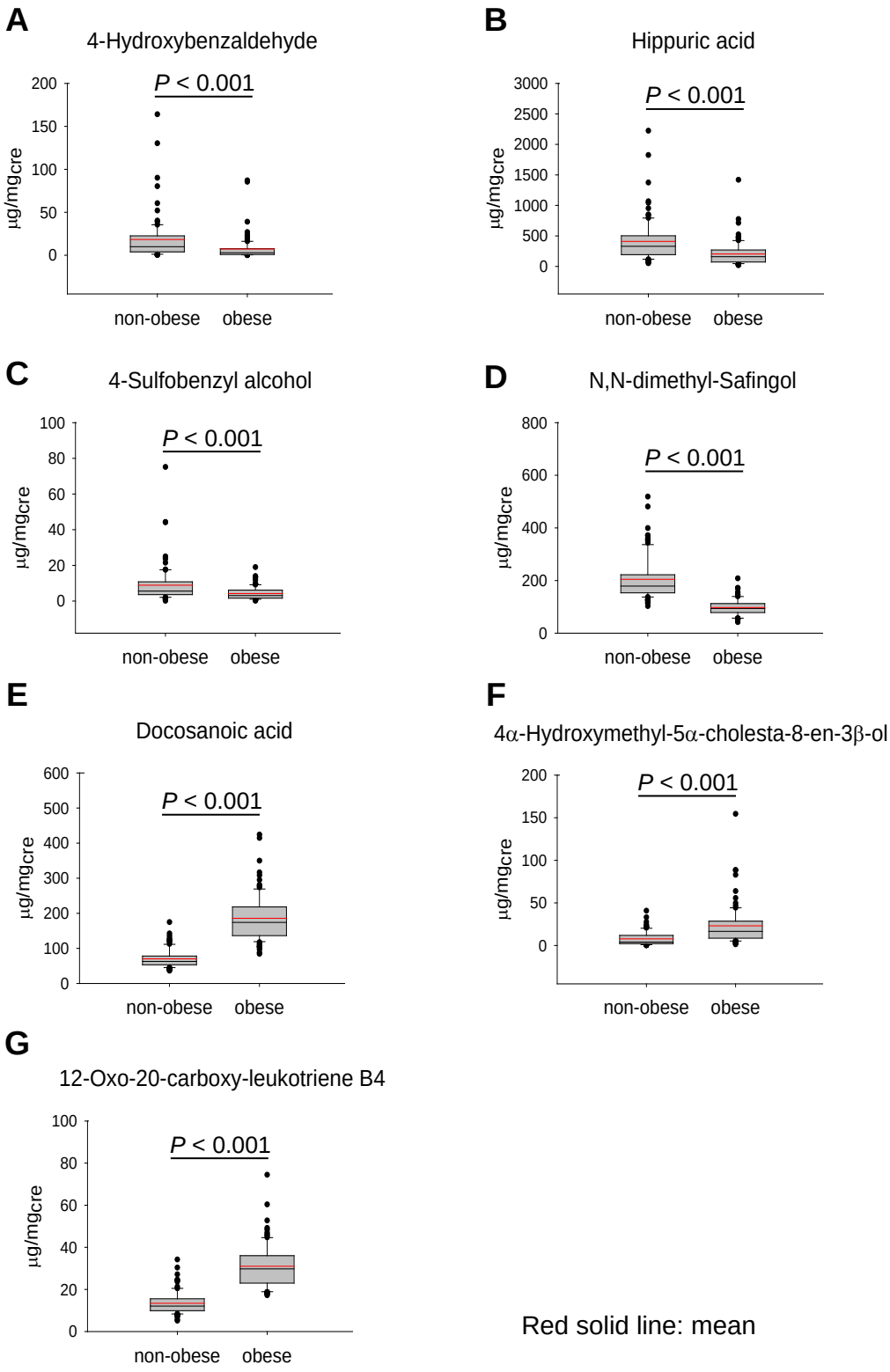
A
4-Hydroxybenzaldehyde
P < 0.001
μg/mgcre
200
150
100
50
0
non-obese
obese
B
Hippuric acid
P < 0.001
μg/mgcre
3000
2500
2000
1500
1000
500
0
non-obese
obese
C
4-Sulfobenzyl alcohol
P < 0.001
μg/mgcre
100
80
60
40
20
0
non-obese
obese
D
N,N-dimethyl-Safingol
P < 0.001
μg/mgcre
800
600
400
200
0
non-obese
obese
E
Docosanoic acid
P < 0.001
μg/mgcre
600
500
400
300
200
100
0
non-obese
obese
F
4α-Hydroxymethyl-5α-cholesta-8-en-3β-ol
P < 0.001
μg/mgcre
200
150
100
50
0
non-obese
obese
G
12-Oxo-20-carboxy-leukotriene B4
P < 0.001
μg/mgcre
100
80
60
40
20
0
non-obese
obese
Red solid line: mean

Figure 3. Box plots of differentially expressed urinary metabolites in the nonobese and obese groups: (A) 4-hydroxybenzaldehyde, (B) hippuric acid, (C) 4-sulfobenzyl alcohol, (D) N,N-dimethyl-safingol, (E) docosanoic acid, (F) 4α-hydroxymethyl-5α-cholesta-8-en-3β-ol, and (G) 12-oxo-20-carboxy-leukotriene B4.

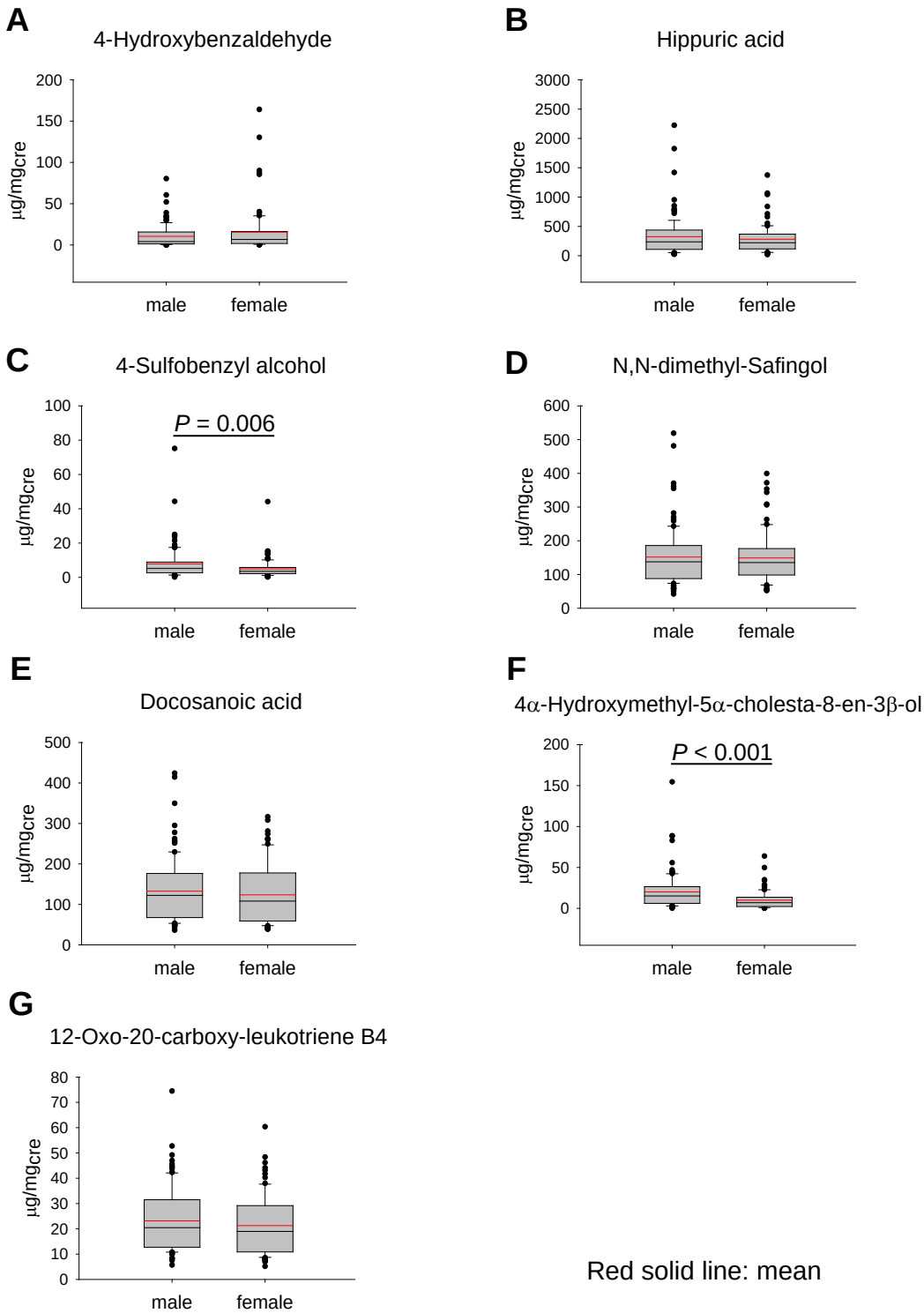
A
4-Hydroxybenzaldehyde
μg/mgcre
200
150
100
50
0
male
female
B
Hippuric acid
μg/mgcre
3000
2500
2000
1500
1000
500
0
male
female
C
4-Sulfobenzyl alcohol
P = 0.006
μg/mgcre
100
80
60
40
20
0
male
female
D
N,N-dimethyl-Safingol
μg/mgcre
600
500
400
300
200
100
0
male
female
E
Docosanoic acid
μg/mgcre
500
400
300
200
100
0
male
female
F
4α-Hydroxymethyl-5α-cholesta-8-en-3β-ol
P < 0.001
μg/mgcre
200
150
100
50
0
male
female
G
12-Oxo-20-carboxy-leukotriene B4
μg/mgcre
80
70
60
50
40
30
20
10
0
male
female
Red solid line: mean

Figure 4. Box plots of differentially expressed urinary metabolites in the male and female groups: (A) 4-hydroxybenzaldehyde, (B) hippuric acid, (C) 4-sulfobenzyl alcohol, (D) N,N-dimethyl-safingol, (E) docosanoic acid, (F) 4α-hydroxymethyl-5α-cholesta-8-en-3β-ol, and (G) 12-oxo-20-carboxy-leukotriene B4.

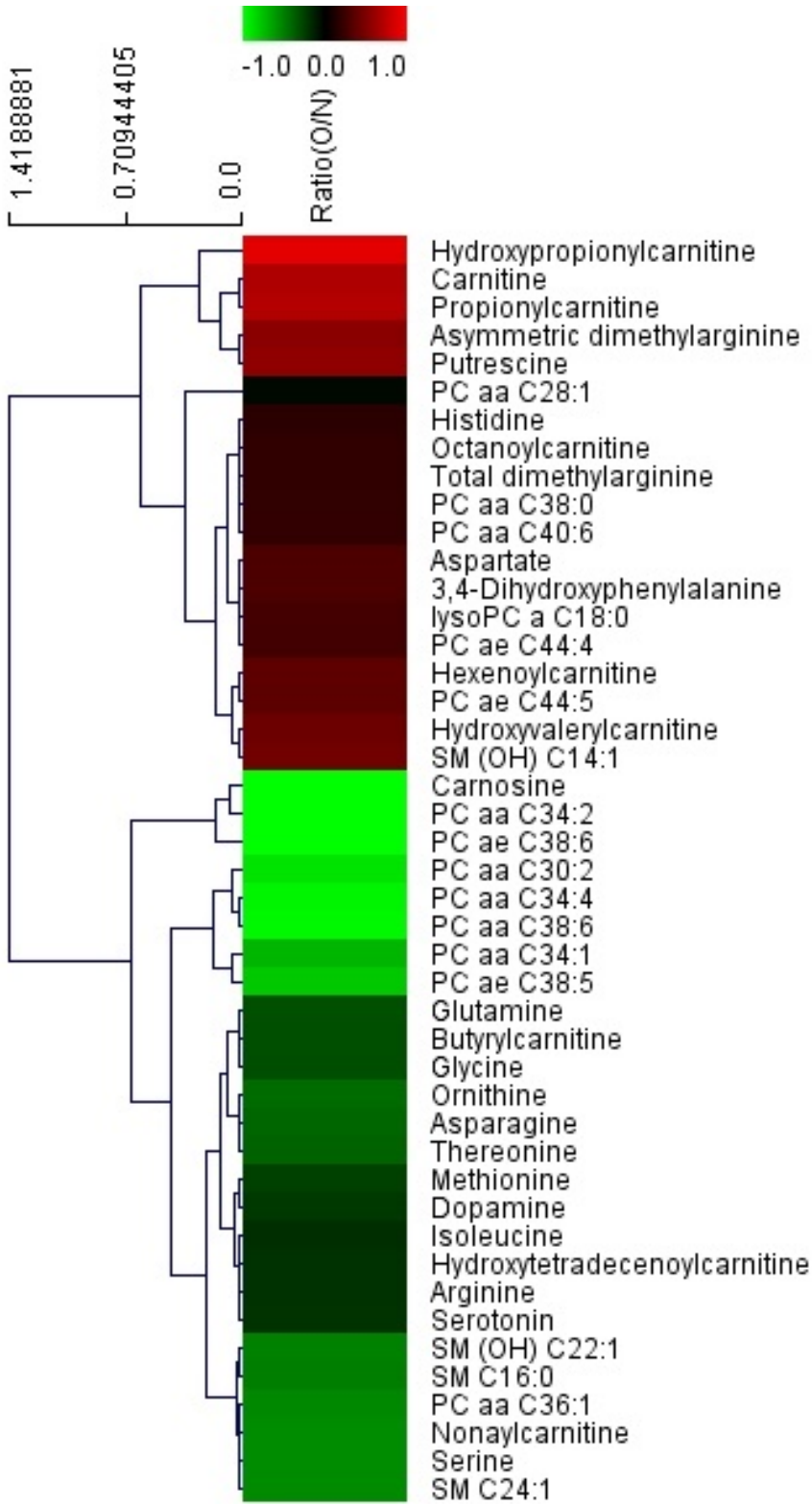
-1.0 0.0 1.0
Ratio(O/N)
1.4188881
0.70944405
0.0
Hydroxypropionylcarnitine
Carnitine
Propionylcarnitine
Asymmetric dimethylarginine
Putrescine
PC aa C28:1
Histidine
Octanoylcarnitine
Total dimethylarginine
PC aa C38:0
PC aa C40:6
Aspartate
3,4-Dihydroxyphenylalanine
lysoPC a C18:0
PC ae C44:4
Hexenoylcarnitine
PC ae C44:5
Hydroxyvalerylcarnitine
SM (OH) C14:1
Carnosine
PC aa C34:2
PC ae C38:6
PC aa C30:2
PC aa C34:4
PC aa C38:6
PC aa C34:1
PC ae C38:5
Glutamine
Butyrylcarnitine
Glycine
Ornithine
Asparagine
Thereonine
Methionine
Dopamine
Isoleucine
Hydroxytetradecenoylcarnitine
Arginine
Serotonin
SM (OH) C22:1
SM C16:0
PC aa C36:1
Nonaylcarnitine
Serine
SM C24:1

Figure 5. Hierarchically clustered heatmap of inflammation-related metabolites in nonobese and obese adolescents. The heatmap was constructed based on the potential candidates of importance that were extracted using t-test analysis and generated by a log2 transformation of the ratio of urinary metabolites in nonobese and obese adolescents. Rows: selected metabolites; columns: expression ratio of obese to nonobese adolescents. The color key indicates the metabolite expression value from red (highest) to green (lowest).

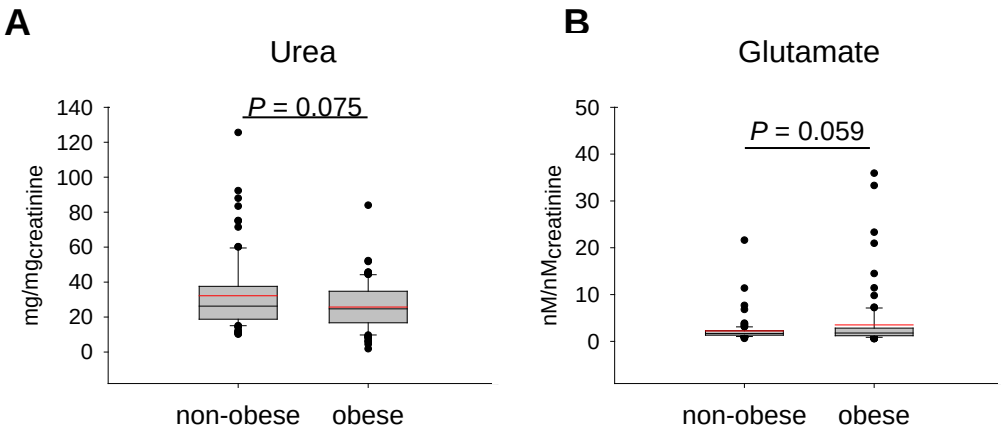

Red solid line: mean

Figure 6. Box plots of (A) urea and (B) glutamate in the nonobese and obese groups.

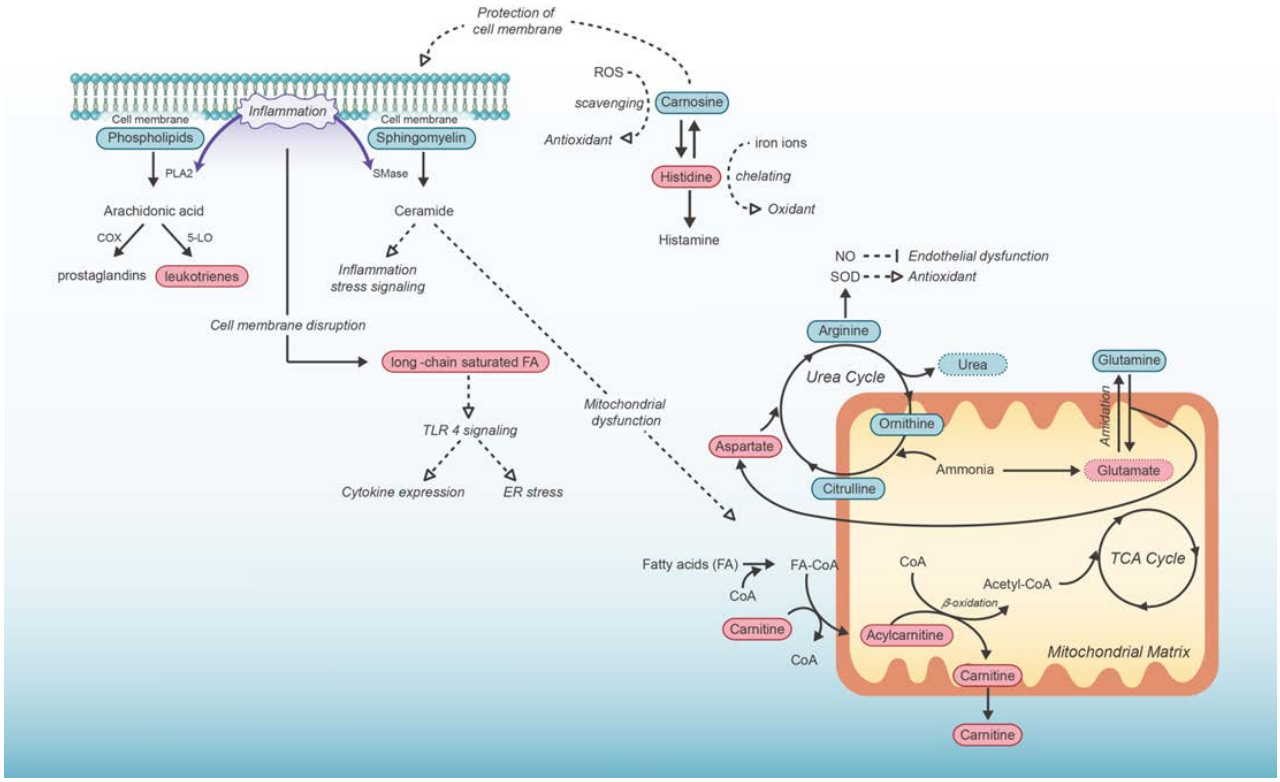
Protection of cell membrane
ROS
scavenging
Carnosine
Antioxidant
iron ions
chelating
Oxidant
Histidine
Histamine
Cell membrane
Inflammation
Cell membrane
Phospholipids
Sphingomyelin
PLA2
SMase
Arachidonic acid
COX
5-LO
prostaglandins
leukotrienes
Ceramide
Inflammation stress signaling
Cell membrane disruption
long -chain saturated FA
TLR 4 signaling
Cytokine expression
ER stress
Mitochondrial dysfunction
NO
Endothelial dysfunction
SOD
Antioxidant
Arginine
Urea Cycle
Urea
Glutamine
Amidation
Ornithine
Aspartate
Ammonia
Glutamate
Citrulline
Fatty acids (FA)
FA-CoA
CoA
Carnitine
CoA
CoA
Acetyl-CoA
TCA Cycle
β-oxidation
Acylcarnitine
Mitochondrial Matrix
Carnitine
Carnitine

Figure 7. Schematic summary of the metabolomics results and explanatory mechanisms. The detected and differentially expressed metabolites are shown by color: solid red oval (increase), solid blue oval (decrease), dotted red oval (increase but not significantly), dotted blue oval (decrease but not significantly). The remaining metabolites were not detected.

Discussion

We revealed urine profiles distinguishing the metabolomic signatures of obese compared to normal weight adolescents using untargeted and targeted metabolomic analyses. Untargeted metabolomics identified differential expression of four metabolites that function in the detoxification of xenobiotics by the microbiome, with 4-hydroxybenzaldehyde, hippuric acid, 4-sulfobenzyl alcohol, and N,N-dimethyl-safingol showing significantly decreased level in obese subjects. Notably, reduced levels of urinary benzoate derivatives and hippuric acid have been consistently reported as an obesity marker in both animal and human studies [19, 20]. Recent studies have suggested that the gut microbiota may impact obesity by regulating energy metabolism through harvesting of energy from the diet, fat storage, lipogenesis and fatty oxidation, modulation of afferent gastrointestinal peptide hormones, and induction of metabolic endotoxemia [21, 22].

Other metabolites associated with inflammation [23-25], i.e., docosanoic acid (behenic acid), 4α-hydroxymethyl-5α-cholesta-8-en-3β-ol (an intermediate in cholesterol biosynthesis), and 12-oxo-20-carboxy-leukotriene B4 (the major metabolite in neutrophil polymorphonuclear leukocytes), were significantly increased in the obese group. During the past decade, studies have shown that inflammation is a key feature of obesity and type 2 diabetes. The endoplasmic reticulum centrally controls cellular metabolism by regulating protein synthesis and secretion and TG and Chol biosynthesis. In the liver, adipose tissue, and pancreas, notable changes in tissue architecture, increases in protein synthesis, and perturbations in cellular energy fluxes occur following inflammation [26]. Furthermore, our results indicated that these three metabolites had high sensitivity and specificity to BMI, AST, ALT, and Chol (Fig. 2B–2E and Table 3) and

suggested that these markers could classify adolescents according to cardiovascular risk as well as obesity.

Subsequently, we performed targeted metabolomics to recognize the metabolomic signatures of obese adolescents using the AbsoluteIDQ p180 kit comprising 186 metabolites reported as markers of various endocrine- or inflammation-related disorders, such as diabetes or cardiovascular diseases. Through MRM analytical platform following sample preparation via the kit, we could identify additional 45 metabolites, including nine acylcarnitines, 11 amino acids, seven biogenic amines, 14 glycerophospholipids, and four sphingolipids, that were altered in obese adolescent urine (Table 4). And we also found that different sample preparation methods and analytical instruments from untargeted metabolomics study may affect resultant metabolites.

Fig. 7 shows a schematic summary of our study using an integrative view of metabolite differences and their related mechanistic pathways: insulin resistance, ammonia toxicity, and oxidative stress.

Insulin resistance

The perception of inflammation in relation to obesity and insulin resistance has been studied since 1993. Many recent studies have shown that highly expressed pro-inflammatory cytokines, such as tumor necrosis factor-α (TNFα) and interleukin-6 (IL-6), suppress insulin signaling pathways in obesity. This suggests that increased levels of inflammation markers may predict future insulin resistance in obese individuals.

In this study, acylcarnitine represented the metabolite showing the greatest increase. Acylcarnitines are known to have a major role in central carbon and lipid metabolism within the mitochondria. Elevated plasma levels of medium-chain (C8, C10, C12, C14) fatty acid-carnitines can arise from incomplete mitochondrial fatty

acid beta-oxidation. Additionally, differences in short-chain (C3, C5) fatty acid-carnitine levels may be positively associated with insulin resistance. Significant correlations exist between incomplete fatty acid oxidation derived acylcarnitines and metabolic disease, including insulin resistance [27]. Therefore, increased urine acylcarnitine levels in obese adolescents may signal an inflammation cascade that features incomplete mitochondrial fatty acid beta-oxidation (Fig. 7).

Conversely, the most decreased metabolites included phospholipids, which have essential structural and functional roles in cell membrane integrity and function. However, various stimuli, such as inflammation, can reduce phospholipid levels and destroy cell membranes (Fig. 7). Furthermore, phospholipid reduction is known to have a positive association with insulin resistance [28]. We also observed that most sphingomyelins (SMs) were decreased. SMs are also membrane constituents, and SM metabolism is related to inflammation and insulin resistance [29] (Fig. 7). Furthermore, SMs may be associated with cardiovascular disorders in obese adolescents. Therefore, increased acylcarnitines and decreased phospholipid and SM levels suggested inflammation and membrane disruption as well as impending insulin resistance in obese adolescents.

Ammonia toxicity

Our study identified statistically significant differences in amino acids, i.e., increased aspartate and decreased arginine and ornithine. These are all constituents of the urea cycle, which is the major route for ammonia detoxification and surplus amino group nitrogen removal in humans [30]. Moreover, urea levels were decreased in obese adolescents, although this difference was not significant (P = 0.075; Fig. 6A). Therefore, increased aspartate and decreased arginine, ornithine, and citrulline could indicate a decrease in urea cycle and ammonia detoxification activity (Fig. 7). Additionally, the amidation of glutamate to glutamine by glutamine synthetase is

another method of ammonia detoxification [31]. In our study, glutamate levels were increased, although this difference was a borderline significant trend (P = 0.059; Fig. 6B). Thus, increased glutamate and decreased glutamine levels could suggest a reduction in ammonia detoxification activity (Fig. 7). Ammonia can be toxic [32] and is thus detoxified via the urea cycle and glutamate amidation; however, Alemany showed that obese individuals could exhibit disruption of nitrogen disposal [33]. In particular, obese individuals were shown to excrete less urea and glutamine than lean individuals, and this could be attributed to urea cycle function and glutamine formation. Our study suggested an alteration in ammonia detoxification processes (i.e., urea cycle and glutamate amidation) in obese individuals, as supported by reduced levels of arginine, ornithine, citrulline, urea, and glutamine and resulting induction of aspartate and glutamate.

Oxidative stress

Among biogenic amines, carnosine (β-alanyl-L-histidine), an antioxidant that scavenges reactive oxygen species (ROS) [34] and efficiently protects the lipid phase of biological membranes and aqueous environments, was significantly decreased. Furthermore, histidine exhibits pro-oxidant activity through active free iron ions [35], and arginine is negatively associated with oxidative stress and inflammation in obese patients [36]. Therefore, increased histidine and decreased carnosine and arginine levels suggest increased oxidative stress in obese adolescents (Fig. 7). Moreover, macronutrient intake may further induce acute oxidative stress by leukocyte-induced ROS [37].

Part II:

Antihyperglycemic mechanism of metformin occurs via the AMPK/LXRα/POMC pathway

Materials and Methods

Subjects and sampling

Fourteen healthy Korean male volunteers participated in the study (aged 20 - 50 years, weighing 50 - 90 kg, and having body mass indexes of 17 - 28 kg/m^2). The study was in accordance with the Declaration of Helsinki and Korea Good Clinical Practice (KGCP) and the protocol and informed consent form were approved by the institutional review board (IRB) of Yonsei University Severance Hospital (4-2009-0334), Seoul, Korea, and each participant gave informed consent for the study. First morning urine samples were collected before and after oral administration of metformin (1000 mg at 8 PM) for metabolomic analyses (Fig. 8).

Metabolomic profiling

A diluted (urine : water = 1 : 4) sample (5 μl) was loaded onto the column held at 40°C and eluted with 0.1% formic acid and 2 mM ammonium formate in water (solvent A), and 0.1% formic acid in methanol (solvent B) over 21 min. While maintaining a constant flow rate of 0.4 ml/min, the metabolites were eluted using the following gradient: 2-98% B from 0.1 to 13 min, and 98% B held constant for 2 min followed by a return to 2% B from 15.1 to 17 min. Chromatographic separations of metabolites in urine were performed with a Zorbax SB-C18, 50 x 2.1 mm, 1.8 μm (Agilent Technologies, Santa Clara, CA) analytical column using an Agilent 1200 series HPLC system (Agilent Technologies, Santa Clara, CA).

The eluent was introduced into Agilent 6530 quadrupole time-of-flight (Q-TOF) mass spectrometer (Agilent Technologies, Santa Clara, CA). The instrument settings were as follows: the nebulizer gas pressure and temperature were 30 psi and 325°C, respectively, and drying gas was set to 11 μl/min. The capillary voltage,

capillary temperature, fragmentor voltage, and skimmer voltage were set to 3.5 kV, 300°C, 170 V, and 65 V, respectively. Centroid data were acquired over an *m/z* range of 100-1,100 using an accumulation time of 0.25 sec per spectrum. The mass accuracy and mass resolution were < 5 parts per million (ppm) and ~ 20,000, respectively. All raw data files were converted to the compound exchange file format using MassHunter DA reprocessor software (Agilent Technologies, Santa Clara, CA).

The overall quality of the analysis procedure was monitored using repeat extracts of a pooled urine sample (QC). To exclude metformin ions from the chromatographic mass data, the parent metformin ion was pursued both in ESI positive mode ($[M + H]^+$ = 130.1087) and ESI negative mode ($[M - H]^-$ = 128.0942) using MassHunter Qualitative Analysis software B.05.00 (Agilent Technologies, Santa Clara, CA), and it was also ensured that no metabolites or conjugates of metformin were present. The metformin ions listed above were removed and Mass Profiler Professional (MPP) software B.12.01 (Agilent Technologies, Santa Clara, CA) was used for aligning data and converting each metabolite feature (m/z × intensity × time) into a matrix of detected peaks versus compound identification. Each sample was normalized to the median of the baseline and log 2 transformed. The MPP software was also employed to perform principal component analysis (PCA) for both positive and negative electrospray ionization (ESI) datasets to evaluate sample clustering according to metformin administration and to identify ions (filtered by following thresholds were presented in volcano plots; fold change $\leq$ 0.5 or fold change $\geq$ 2, and $P < 0.05$).

The resulting metabolites were identified using the human metabolome database (HMDB), METLIN, and the MS/MS fragment pattern with pure analytical standards. Finally, the metabolites were quantified by normalization to urinary creatinine concentrations.

Cell lines and cell culture

The rat pituitary adenoma cell line GH3 was obtained from the Korean Cell Line Bank (Seoul, Korea). The pituitary adenoma cell line was authenticated by the suppliers by DNA profiling and cytogenetic analysis and in our laboratory by morphology and growth rate. Cells were grown under 5% CO_2 at 37°C in Dulbecco's modified Eagle's medium supplemented with 10% fetal bovine serum (FBS), which was purchased from Sigma–Aldrich (St. Louis, MO, USA), along with other chemicals.

Small interfering RNA (siRNA)-mediated gene silencing

For transient transfection with siRNAs, 40% confluent cells were transfected with negative control siRNA vector or two different siRNAs using Lipofectamine RNAiMAX reagents (Life Technologies, Grand Island, NY, USA). The transfected cells were allowed to stabilize for 36–48 h before being used in experiments.

Animal experiments

Four-week-old male rats were randomly divided into the control or test group. Then, PBS or metformin (20 mg/kg; Sigma-Aldrich, St. Louis, MO) in PBS was administered intraperitoneally once-daily for 3 consecutive days to control or test groups, respectively. The dose (20 mg/kg) and treatment period (3 days) of metformin was determined considering the previous reports, which described that rodents need higher doses or longer period of metformin treatment than human due to the different drug sensitivity among species [14,38-40]. Rats were individually housed for 1 week prior to a 3-day acclimation period in the metabolic cages, and assessed for 3 days while fed a chow diet. Since rats are nocturnal animals that have the physiology during the day corresponds to the human physiology at night,

we collected evening urine samples comparable to the morning sample to human [41]. The rats were euthanized with inhaled isoflurane and their pituitaries were removed and fixed in 4% paraformaldehyde overnight (Fig. 17).

Urinary cortisol levels were measured using a 12-chamber metabolic chamber system at the Institute for Experimental Animals (Seoul National University College of Medicine, Republic of Korea).

Enzyme-linked immunosorbent assays (ELISA)

Urinary ACTH concentrations were measured using ELISA kits (MyBioSource, Inc., San Diego, CA).

Western blot analysis

To quantify protein levels, equal amounts of total protein were loaded into lanes and separated on SDS-polyacrylamide gels. The gels were transferred to Immobilon-P membranes (Millipore, Billerica, MA, USA) and the membranes were then blocked with 5% nonfat milk in Tris-buffered saline containing 0.05% Tween 20 (TTBS) at room temperature for 1 h and incubated overnight at 4°C with a primary antibody diluted 1:1000 to 1:5000 in 5% nonfat milk in TTBS. The primary antibodies used were antisera against AMPK and p-AMPK (Cell Signaling, Danvers, MA, USA), LXRα (Abcam, Cambridge, UK), and POMC (Novus Biologicals, Littleton, CO, USA). Horseradish peroxidase-conjugated anti-rabbit or anti-goat antiserum was used as a secondary antibody (1:5000), and antigen-antibody complexes were visualized using an Enhanced Chemiluminescence Plus Kit (GE Healthcare, UK), followed by exposure to X-ray film.

Immunoprecipitation

Cell lysates were incubated with 5 μl of anti-phospho-Threonine antiserum (Cell Signaling, Danvers, MA, USA), or preimmune serum at 4°C for 16 h. Immune complexes were further incubated with protein A/G-Sepharose beads (GE Healthcare, UK) at 4°C for 2 h. Immunocomplexes were eluted by boiling for 10 min in a sample buffer containing 2% SDS and 10 mM dithiothreitol, separated on SDS-polyacrylamide gels, and then immunoblotted using anti-LXRα antibody.

Immunohistochemistry (IHC)

Paraffin-embedded pituitary sections (4 μm) were rehydrated and autoclaved at 121°C for 10 minutes in 100 mM citrate buffer (pH 6.0) for retrieving antigens prior to staining. The sections were then treated with 3% hydrogen peroxide for 30 min and with 10% bovine serum for 2 h to block nonspecific binding. They were then incubated with antibodies against p-AMPK (1:20; Cell Signaling Technology, Danvers, MA, USA), POMC (1:100; Novus Biologicals, Littleton, CO, USA), ACTH (1:100; Novus Biologicals, Littleton, CO, USA), LXRα (1:50; Santa Cruz Biotechnology, Santa Cruz, CA, USA), or LXRβ (1:50; Santa Cruz Biotechnology, Santa Cruz, CA, USA) over night at 4°C. Biotinylated secondary antibodies (Vector laboratories, Burlingame, CA, USA) were used for staining p-AMPK (1:50), POMC (1:200), ACTH (1:200), LXRα (1:200), or LXRβ (1:200). The immune complexes were visualized using the Vectastain ABC kit (Vector Laboratories, Burlingame, CA). Negative controls were performed using IgG isotype antibodies (eBioscience, San Diego, CA). To standardize color development, the incubation time for diaminobenzidine staining was fixed in all experiments. All immunostained sections were lightly counterstained with hematoxylin. The slides were evaluated with a bright-field microscope (BX-51; Olympus, Tokyo, Japan) equipped with a camera (DP70; Olympus, Tokyo, Japan)

and a micrograph field of view of the entire stained section. Relative intensities of stained targets were calculated using ImageJ v1.47 (NIH, USA).

Statistical analysis

All data were analyzed using IBM SPSS Statistics 19 (Chicago, IL, USA), and results are expressed as means and standard deviations. Data were statistically analyzed using the Wilcoxon signed ranks test, Pearson correlation, and linear regression. Differences were considered significant when P was < 0.05 in two-tailed statistics.

Results

In this study, 14 healthy subjects were administered metformin once orally, and first morning urine samples were obtained before and after treatment. The samples were analyzed by HPLC/Q-TOF MS and further by multivariate data analysis. Principal component analysis (PCA) revealed a clear discrimination between the control (*blue*) and metformin-treated group (*red*) in both ESI (+) and (−) modes, which indicates that metformin could affect the endogenous metabolomic profiles in urine (Fig. 9).

The urine levels of several endogenous metabolites were changed significantly by orally administrated metformin (Fig. 10 and Table 5). Especially, four metabolites including cortisol, retinyl β-glucuronide, betaine, and cholic acid glucuroninde were identified with pure analytical standards, and finally quantified by normalization for urinary creatinine (Fig. 11). Among them, cortisol was significantly decreased and its metabolite hydroxycortisol also decreased after metformin administration, although this difference was a borderline significant trend (Fig. 12A and 12B). Also most subjects' levels of cortisol were decreased (Fig. 13A). Cortisol is a well-known stress hormone, and plays key roles in stimulating gluconeogenesis by breaking down of glycogen to glucose-1-phosphate and glucose [42]. Given that cortisol has been known that which is closely related to the glucose levels, we further studied how cortisol effects on antiglycemic action of metformin.

Since the single treatment of metformin rapidly affects cortisol levels, we then observed the neuroendocrine response to metformin. Previous studies have examined enhanced HPA axis activity in patients with type 2 diabetes [43,44]. However, given that metformin is prescribed primarily as an antidiabetic drug, its

role in the HPA axis and related mechanisms is not clear. Thus, we hypothesized that reduced cortisol was related to the antidiabetic function of metformin. At first, considering that ACTH regulates secretion of cortisol by stimulating the adrenal cortex, we measured urinary ACTH concentrations in human subjects groups by using ELISA analysis. The urinary ACTH concentrations were decreased by 11% in metformin administered group (Fig. 12C). In addition, the changes in cortisol and ACTH levels correlated significantly with each other (Fig. 12E). Furthermore, glucose levels were also decreased (Fig. 12D). These data showed that metformin could reduce ACTH and cortisol secretion as well as glucose level. To further investigate how metformin reduces cortisol through the neuroendocrine system, we evaluated key elements of the HPA axis *in vitro* and *in vivo* after metformin treatment.

Matsumoto et al. recently reported that pituitary LXRα plays an important role in cortisol levels through the regulation of POMC and ACTH by the LXR agonist in mice. In particular, they showed that LXRα directly regulates the POMC gene promoter, indicating that POMC gene expression is positively regulated by LXRα at the transcriptional level [45]. Also, Hwahng et al. reported that AMPK phosphorylated LXRα at threonine residues has an inhibitory effect on those downstream genes [46]. Thus, we measured threonine phosphorylated LXRα and found that the inhibitory phosphorylation is upregulated in the presence of metformin (Fig. 14C), although total LXRα expression was not changed, at the dose and time when AMPK was fully activated (Fig. 14A). A recent report on metformin quantification in the rat brain found that orally-dosed metformin rapidly crossed the blood-brain-barrier (BBB) and affected POMC (a precursor of ACTH) expression in the pituitary as well as ACTH-stimulated cortisol levels in blood [15]. In addition, other researchers stated that metformin activates AMPK in rat pituitary cells [13]. Here, we also found metformin induced AMPK activation and POMC

reduction in rat pituitary adenoma cells (Fig. 14A and 14B). Using knockdown techniques, we found out that metformin-induced POMC reduction is dependent on AMPK and LXRα activation (Fig. 14D and 14E); however, metformin induced AMPK activation occurs independently from LXRα phosphorylation (Fig. 14E). This result indicated that metformin induced AMPK activation reduces POMC expression through LXRα inhibitory phosphorylation in the pituitary.

To evaluate the *in vivo* effects of metformin on cortisol reduction through the AMPK/LXRα/POMC pathway, we administered metformin to rats in this study. We verified that p-AMPK, POMC, and ACTH expression levels were significantly altered in the pituitary glands of rats (Fig. 18A), and the urinary cortisol levels also decreased after administration of metformin (Fig. 18B). The protein expression of p-AMPK increased, while POMC and ACTH expression decreased in the metformin-administered group. We also confirmed, with immunostaining, LXRα and LXRβ in the pituitary by using antibodies specific to each of them (Fig. 19). Using immunohistological analysis of the rat pituitary, we elucidated that the number of LXRα immunoreactive cells was greater than that of LXRβ reactive cells, and that the role of LXRα is critical in the pituitary. These results are supported by a study that found LXRα is more highly expressed than LXRβ in the pituitary and directly regulates POMC at the transcriptional level [45]. We also found the rat urinary cortisol and glucose levels were not changed in the PBS treatment group (data not shown); however, they changed significantly in the metformin treatment group, similar to in humans (Fig. 18B and 18C). Therefore, metformin induced ACTH reduction via the AMPK/LXRα/POMC pathway, and simultaneously reduced cortisol and glucose *in vivo* (Fig. 20).

Table 5. Chemically identified metabolites in urine specimens collected from metformin-treated subjects and untreated subjects.

Ion mode	t_R (min)	Observed mass (*m/z*)	Formula	Fold change	*p*-value	Identity	Super class
ESI+	0.52	118.0863	$C_5H_{11}NO_2$	0.64	0.0398	Betaine	Amino acids
	3.0	161.1074	-	3.0	0.0006	*(unidentified)*	-
	7.0	363.2166	$C_{21}H_{30}O_5$	0.73	0.0003	Cortisol	Lipids
	8.5	463.2676	$C_{26}H_{38}O_7$	2.0	0.0391	Retinyl β-glucuronide	Lipids
ESI-	1.3	245.1139	-	1.8	0.0245	*(unidentified)*	-
	2.9	279.0980	-	1.5	0.0329	*(unidentified)*	-
	9.7	583.3124	$C_{30}H_{48}O_{11}$	1.6	0.0083	Cholic acid glucuronide	Lipids

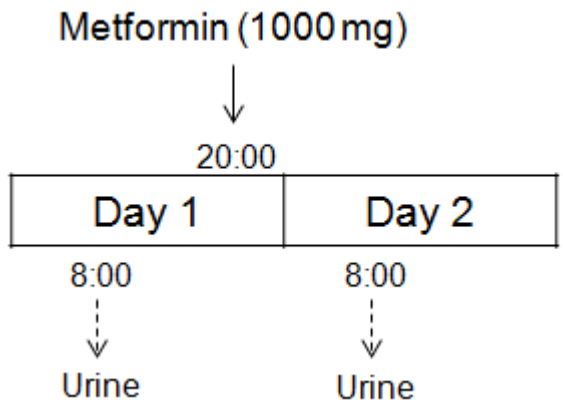
Metformin (1000 mg)
20:00
Day 1
Day 2
8:00
8:00
Urine
Urine

Figure 8. A schedule of metformin administration and urine collection in human study.

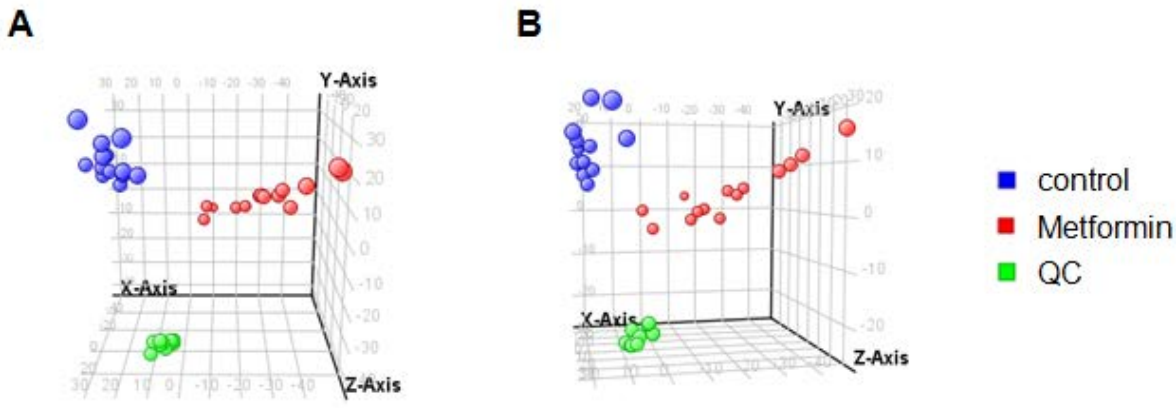
A
Y-Axis
X-Axis
Z-Axis
B
Y-Axis
X-Axis
Z-Axis
control
Metformin
QC

Figure 9. Untargeted metabolomic profiling using HPLC/Q-TOF MS generated PCA score plots discriminating the metformin treated healthy subjects group (*red*) from the control group (*blue*). QCs are for monitoring the overall quality of the analysis procedure (*green*). Data are shown for (A) the positive and (B) the negative ESI datasets.

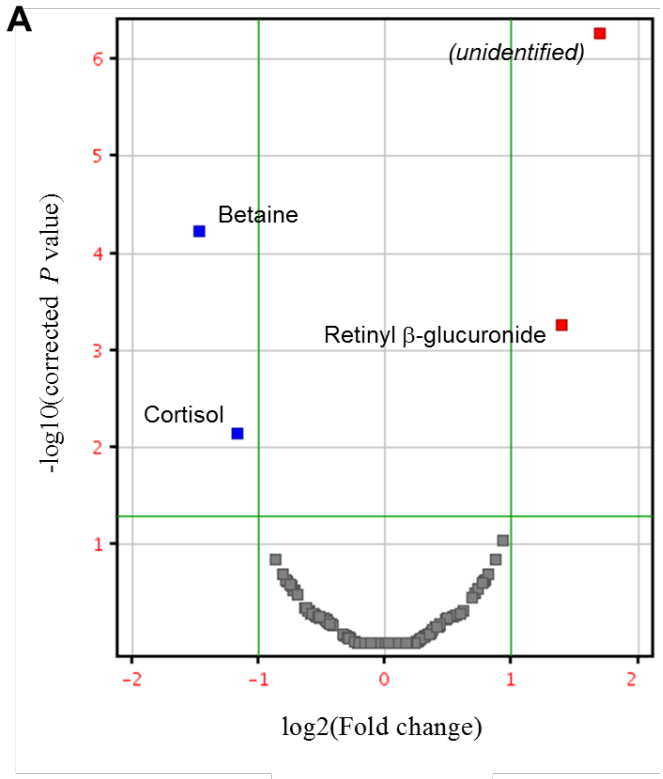
A
(unidentified)
Betaine
Retinyl β-glucuronide
Cortisol
-log10(corrected P value)
log2(Fold change)
6
5
4
3
2
1
-2
-1
0
1
2

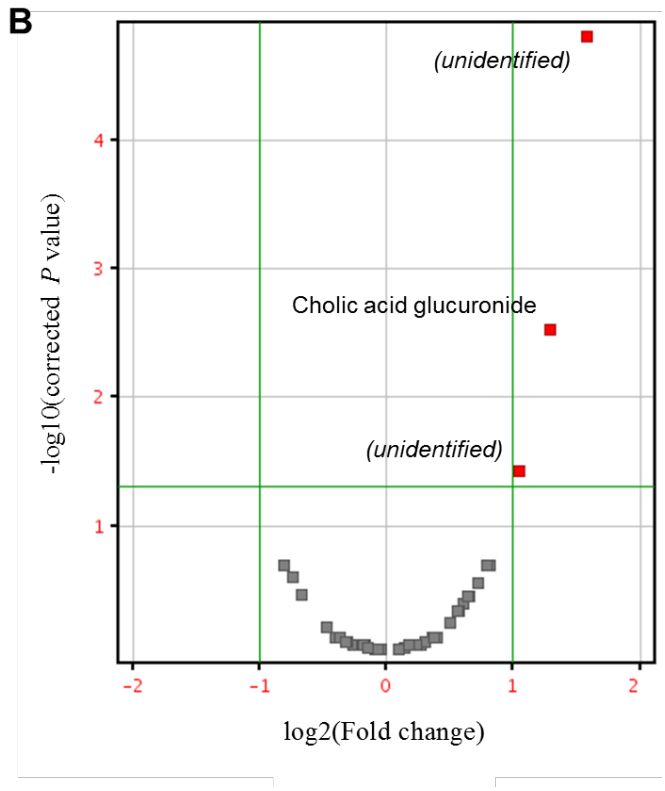
B
(unidentified)
Cholic acid glucuronide
(unidentified)
-log10(corrected P value)
log2(Fold change)
4
3
2
1
-2
-1
0
1
2

Figure 10. Volcano plots showing metabolites discriminating the metformin treated healthy subjects group from the control group. Data are shown for (A) the positive and (B) the negative ESI datasets.

A

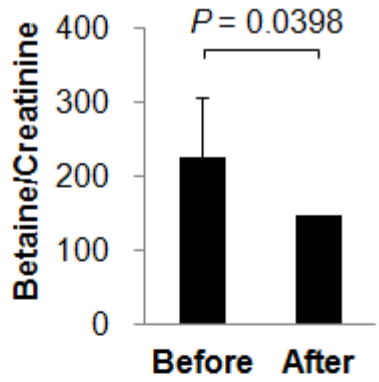
P = 0.0398
Betaine/Creatinine
400
300
200
100
0
Before
After

B

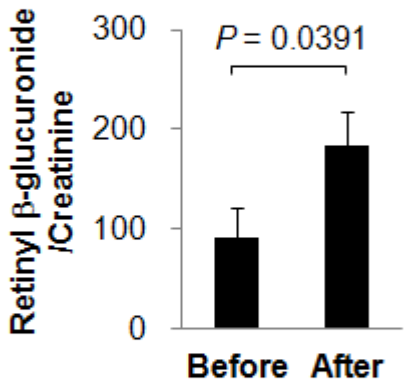
P = 0.0391
Retinyl β-glucuronide /Creatinine
300
200
100
0
Before
After

C

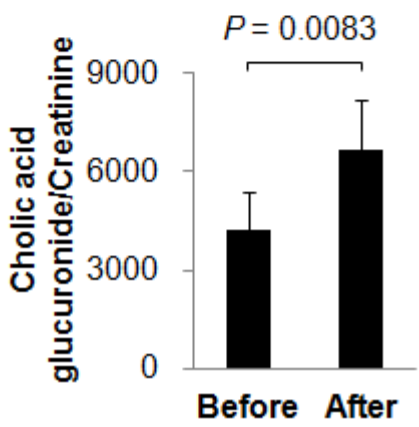
P = 0.0083
Cholic acid glucuronide/Creatinine
9000
6000
3000
0
Before
After

Figure 11. Quantification of identified urinary metabolites in healthy subjects before and after metformin (1000 mg) administration. The normalized urinary concentrations of (A) betaine and (B) retinyl β-glucuronide from ESI+ mode, and of (C) cholic acid glucuronide from ESI- mode. Data are expressed as the mean ± SE. A representative data from 3 independent experiments.

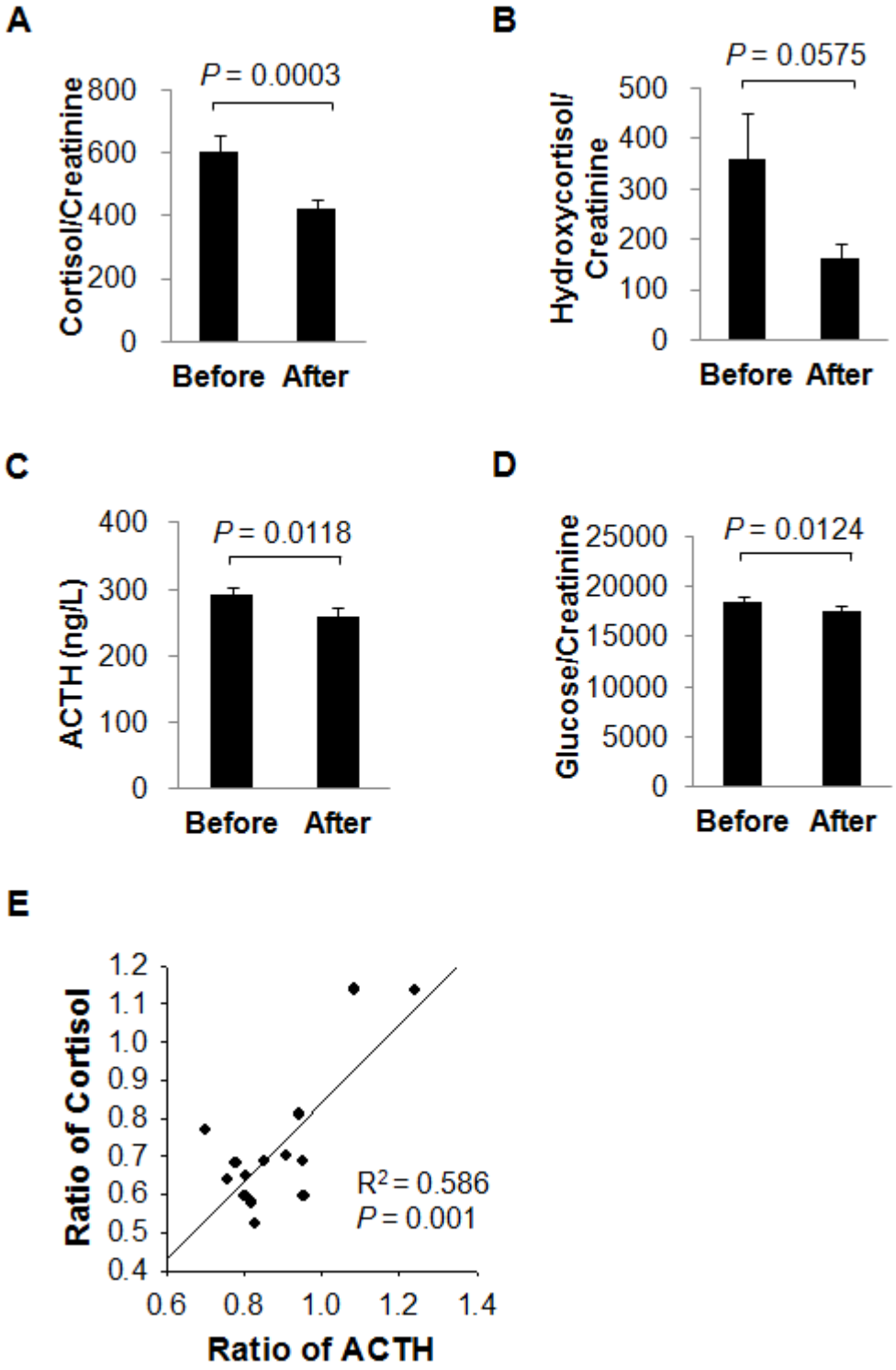
A
P = 0.0003
Cortisol/Creatinine
800
600
400
200
0
Before
After
B
P = 0.0575
Hydroxycortisol/
Creatinine
500
400
300
200
100
0
Before
After
C
P = 0.0118
ACTH (ng/L)
400
300
200
100
0
Before
After
D
P = 0.0124
Glucose/Creatinine
25000
20000
15000
10000
5000
0
Before
After
E
Ratio of Cortisol
1.2
1.1
1.0
0.9
0.8
0.7
0.6
0.5
0.4
R² = 0.586
P = 0.001
0.6
0.8
1.0
1.2
1.4
Ratio of ACTH

Figure 12. Metformin reduces urinary cortisol, hydroxyl cortisol, ACTH, and glucose levels in the subjects. For quantification, (A) cortisol and its metabolite (B) hydroxycortisol, (C) ACTH, and (D) glucose levels were normalized to those of creatinine. Levels of ACTH were measured by ELISA. Data are expressed as the mean ± SE. (E) Correlation between the ratio of cortisol and ACTH levels showed that metformin reduced ACTH secretion and cortisol levels.

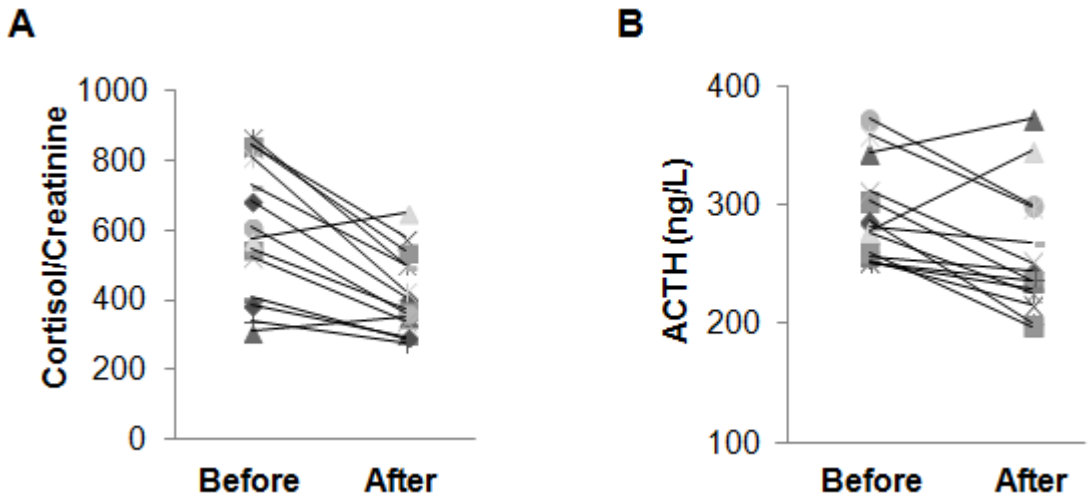
A
Cortisol/Creatinine
1000
800
600
400
200
0
Before
After
B
ACTH (ng/L)
400
300
200
100
Before
After

Figure 13. Spaghetti plots for individual subject's urinary (A) cortisol and (B) ACTH levels. A representative data from 3 independent experiments.

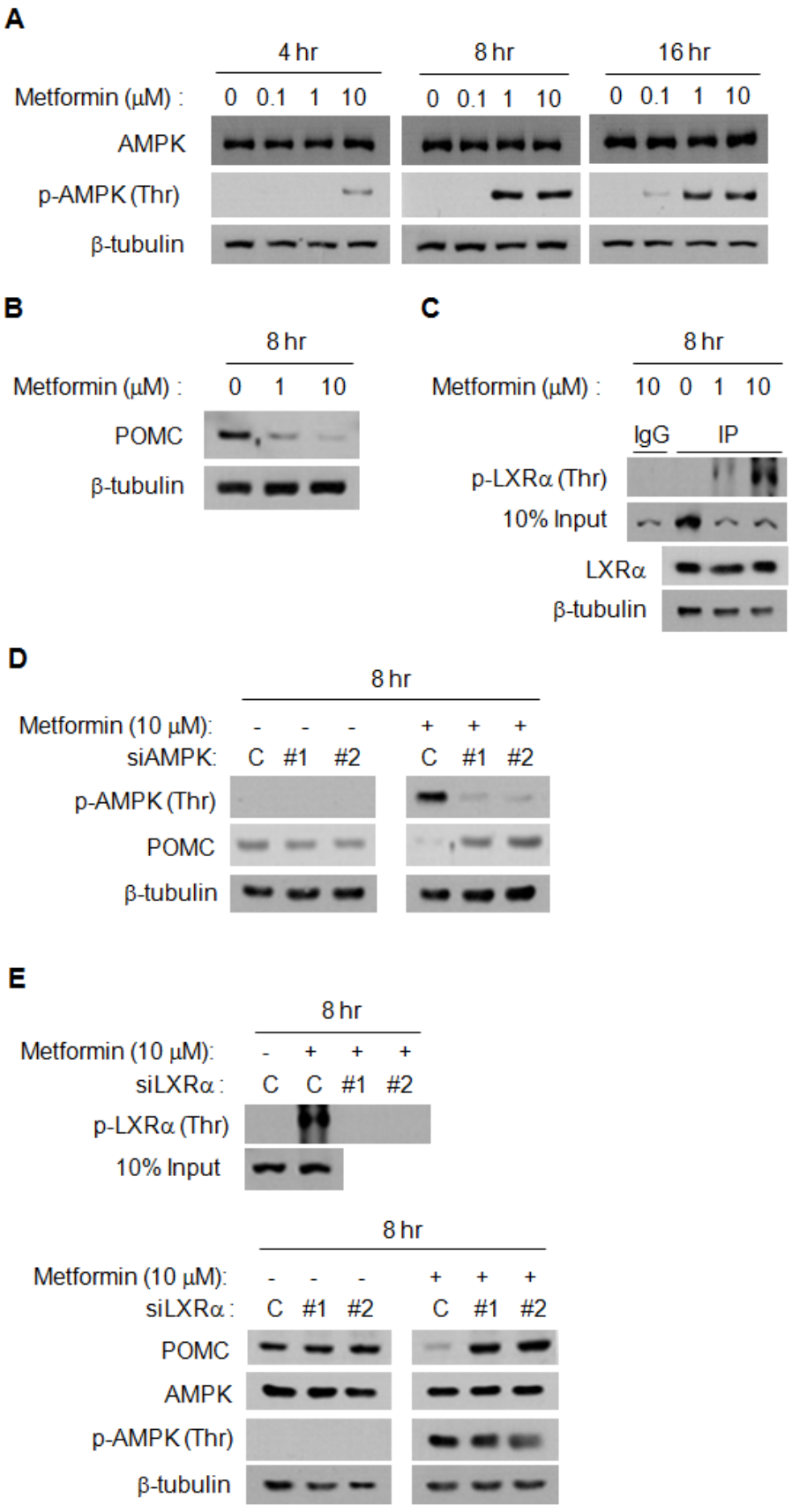
A
4 hr
8 hr
16 hr
Metformin (μM) :
0 0.1 1 10
0 0.1 1 10
0 0.1 1 10
AMPK
p-AMPK (Thr)
β-tubulin
B
8 hr
Metformin (μM) :
0 1 10
POMC
β-tubulin
C
8 hr
Metformin (μM) :
10 0 1 10
IgG
IP
p-LXRα (Thr)
10% Input
LXRα
β-tubulin
D
8 hr
Metformin (10 μM):
- - - + + +
siAMPK:
C #1 #2 C #1 #2
p-AMPK (Thr)
POMC
β-tubulin
E
8 hr
Metformin (10 μM):
- + + +
siLXRα :
C C #1 #2
p-LXRα (Thr)
10% Input
8 hr
Metformin (10 μM):
- - - + + +
siLXRα :
C #1 #2 C #1 #2
POMC
AMPK
p-AMPK (Thr)
β-tubulin

Figure 14. Metformin suppresses POMC protein levels through phosphorylation of AMPK and subsequently LXRα *in vitro*. The rat pituitary adenoma GH3 cells were treated with metformin by using the indicated concentrations and treatment times, and total cell lysates were used for western blotting. (A and B) Metformin upregulated AMPK phosphorylation and downregulated POMC expression. (C) Total cell lysates were used for immunoprecipitation with anti-phopho-Thr antibody and western blotting with anti-LXRα antibody. (D) Reduced POMC after metformin treatment was restored when two siRNAs (#1 and #2) targeting AMPK were transfected in GH3 cells. (E) After metformin treatment, knockdown of LXRα by using two siRNAs (#1 and #2) targeting LXRα (*upper*) restored POMC expression, although p-AMPK was still enhanced (*lower*).

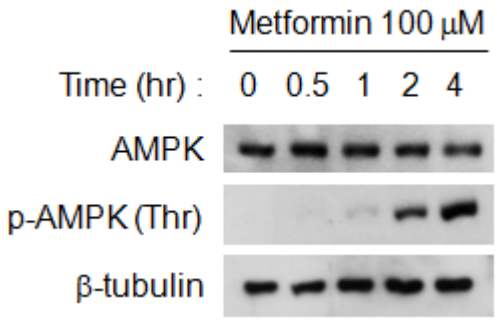
Metformin 100 μM
Time (hr) : 0 0.5 1 2 4
AMPK
p-AMPK (Thr)
β-tubulin

Figure 15. Metformin showed acute phosphorylation of AMPK. The rat pituitary adenoma GH3 cells were treated with metformin by concentration at 10 times higher (100 μM) than we used in main Figures. A representative data from 3 independent experiments.

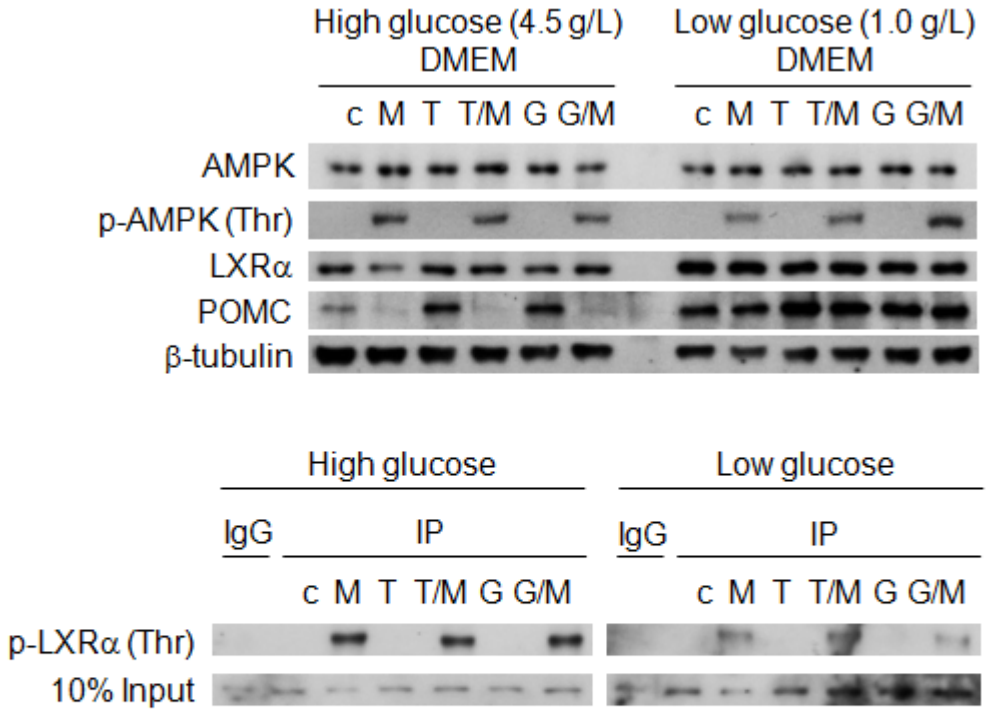

c: control (DMSO)
M: Metformin (10 uM)
T: T0901317 (10 uM)
G: GW3965 hydrochloride (10 uM)

Figure 16. Metformin regulates POMC differently according to the glucose concentration. The rat pituitary adenoma GH3 cells were treated with LXRα agonist either T0901317 (T) or GW3965 hydrochloride (G) or with or without metformin for 8 hours, and total cell lysates were used for western blotting. Metformin upregulated AMPK phosphorylation in both high glucose and low glucose media, however, POMC expressions were different under high or low glucose media condition (*upper).* Total cell lysates were used for immunoprecipitation with anti-phopho-Thr antibody and western blotting with anti-LXRα antibody (*lower*). A representative data from 3 independent experiments.

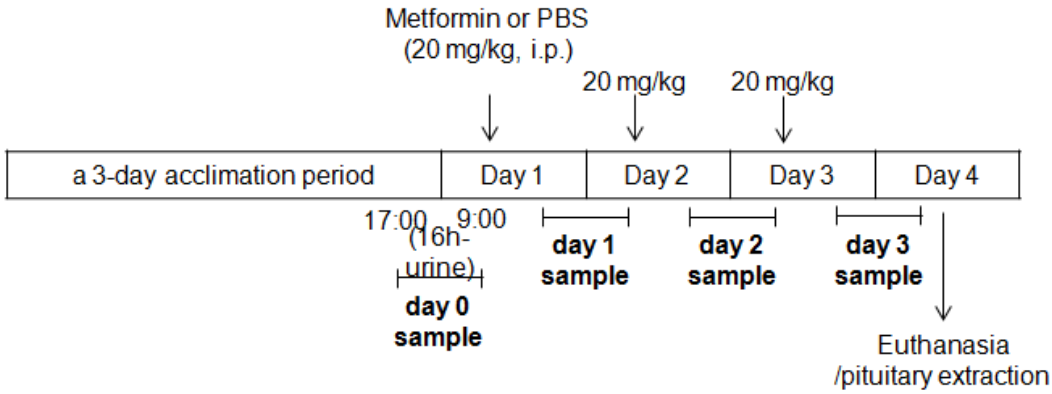
Metformin or PBS
(20 mg/kg, i.p.)
20 mg/kg
20 mg/kg
a 3-day acclimation period
Day 1
Day 2
Day 3
Day 4
17:00
9:00
(16h-urine)
day 0 sample
day 1 sample
day 2 sample
day 3 sample
Euthanasia /pituitary extraction

Figure 17. The design of rat experiments: a schedule of metformin administration, urine collection, and pituitary extraction.

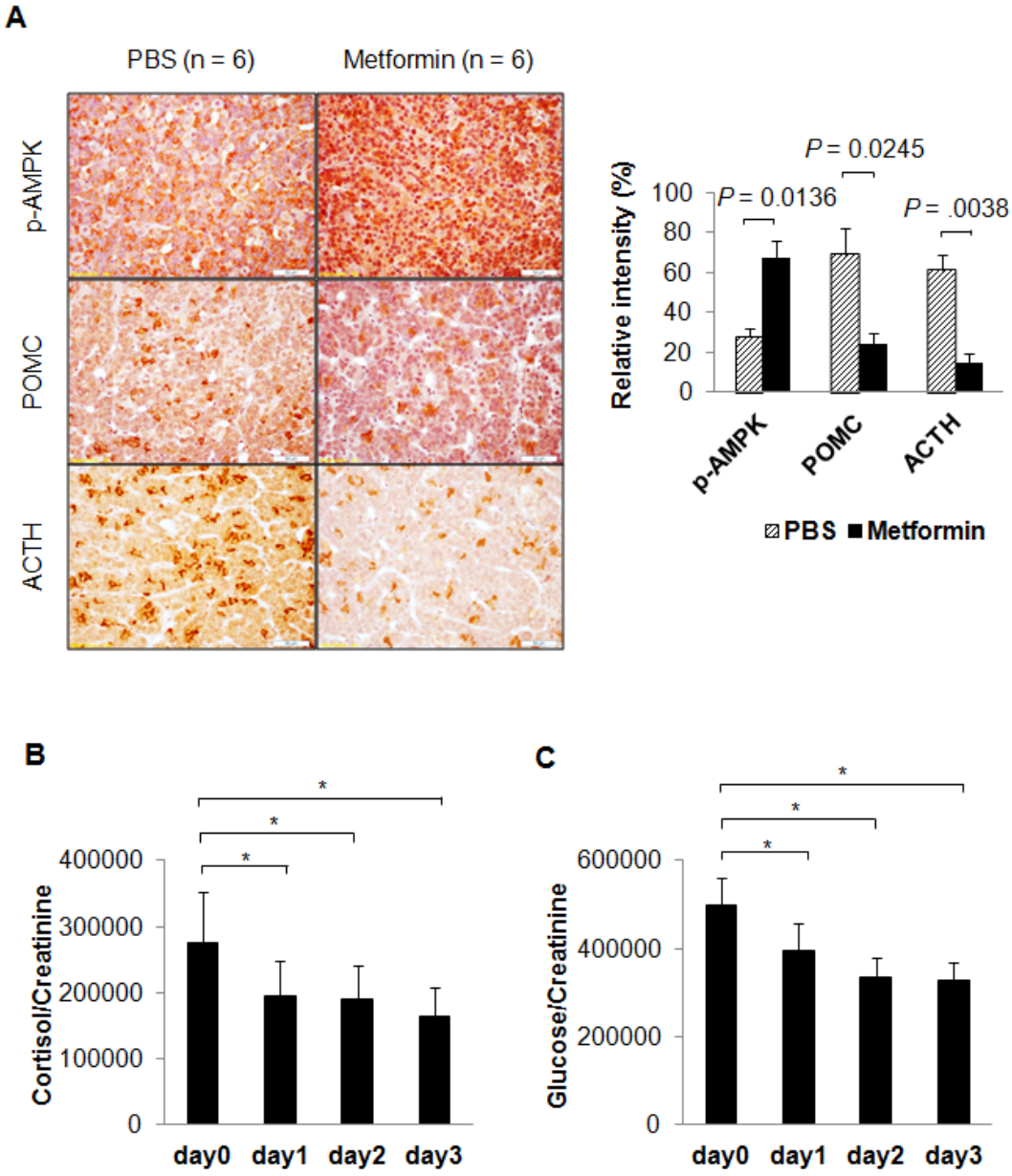
A
PBS (n = 6)
Metformin (n = 6)
p-AMPK
POMC
ACTH
Relative intensity (%)
P = 0.0245
P = 0.0136
P = .0038
100
80
60
40
20
0
p-AMPK
POMC
ACTH
PBS
Metformin
B
Cortisol/Creatinine
400000
300000
200000
100000
0
day0
day1
day2
day3
C
Glucose/Creatinine
600000
400000
200000
0
day0
day1
day2
day3

Figure 18. Metformin activates AMPK and reduces POMC, ACTH, cortisol, and glucose levels *in vivo*. (A) Immunohistochemical staining (*dark brown*) of paraffin-embedded pituitary sections showed metformin (20 mg/kg) induced AMPK phosphorylation, and inhibited POMC and ACTH expression (*left*). The images are of a representative section (original magnification, ×400. Bar, 50 μm). The number of cells immunoreactive for p-AMPK, POMC, or ACTH was normalized to the total number of cells (*right*). Data represent the mean ± SE (n = 6). Relative quantification of the creatinine normalized urinary (B) cortisol and (C) glucose in rats before and after metformin treatment (once-daily for 3 consecutive days). Data are expressed as the mean ± SE.

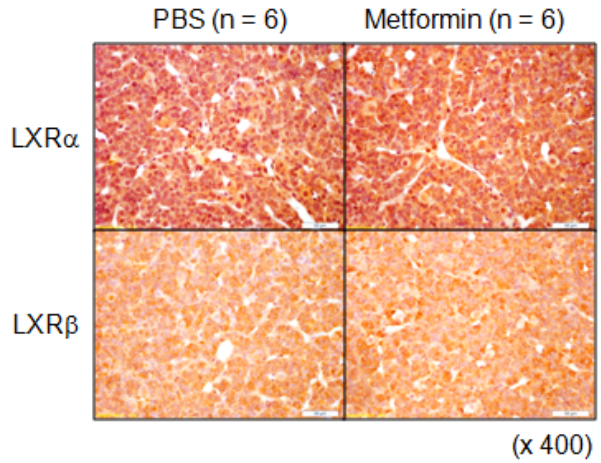
PBS (n = 6)
Metformin (n = 6)
LXRα
LXRβ
(x 400)

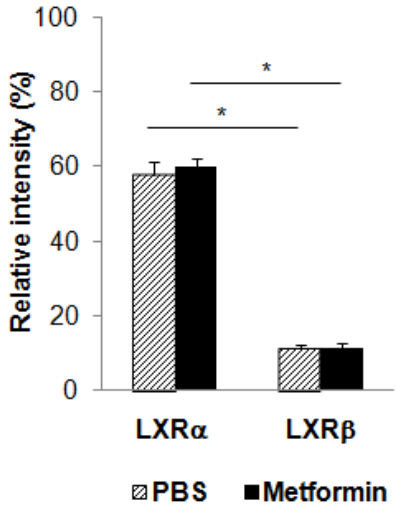
Relative intensity (%)
100
80
60
40
20
0
*
*
LXRα
LXRβ
PBS
Metformin

* $P < 0.0001$

Figure 19. Expression levels of LXRα and LXRβ after metformin treatment *in vivo*. LXRα and LXRβ expression levels in the metformin treatment group were comparable to the control groups. The images are of a representative section (original magnification, ×400. Bar, 50 μm) (*upper*). The number of cells immunoreactive for LXRα and LXRβ was normalized to the total number of cells. Data represent the mean ± SE (n = 6) (*lower*).

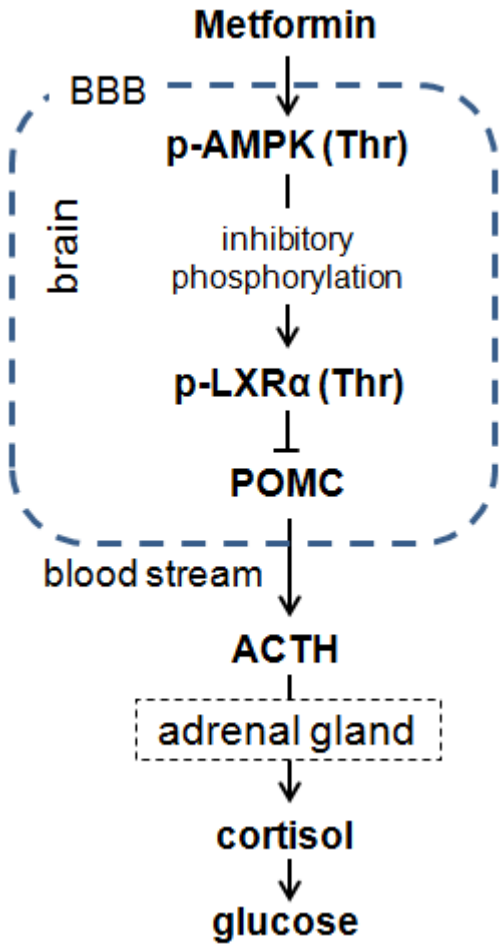
Metformin
BBB
p-AMPK (Thr)
brain
inhibitory
phosphorylation
p-LXRα (Thr)
POMC
blood stream
ACTH
adrenal gland
cortisol
glucose

Figure 20. Proposed mechanism of the antihyperglycemic action of metformin via the AMPK/LXRα/POMC pathway.

Discussion

We found that several urine metabolites were significantly changed in metformin administered healthy subjects using metabolomic analysis. This urinary metabolomics study determined the endogenous metabolites affected by metformin administration. Among them, retinyl β-glucuronide and cholic acid glucuronide are conjugates of metabolites of retinol and bile acid, respectively. Given that retinol and bile acid induce liver toxicity [47,48], we considered that increased glucuronidation of them provides clues about the potential detoxifying role of metformin. Furthermore, recent studies stated that metformin could treat chronic liver diseases by protecting against bile acid induced apoptosis [49]. Another metabolite found, betaine, is known to lower homocysteine levels in blood as an antioxidant [50]. Given that metformin treatment elevates homocysteine levels, even under short-term treatment conditions, we inferred that reduced levels of betaine have causative effects on metformin induced oxidative stress [51,52]. However, the clinical significance of these findings remains to be further investigated. Finally, we identified cortisol, a well-known stress hormone that is secreted from the adrenal cortex and stimulated by adrenocorticotropic hormone (ACTH) through a major part of the neuroendocrine system hypothalamic-pituitary-adrenal (HPA) axis. Surprisingly, our data showed that urinary cortisol, its metabolite hydroxycortisol, and ACTH levels were decreased after metformin administration, and all participants except two subjects showed the decreased cortisol and ACTH levels (Fig. 13A and 13B).

Several studies reported that AMPK activation by either adiponectin or AICAR increased POMC expression or ACTH level. Iwasaki et al stated that AMPK activation by AICAR increased the activity of POMC gene [53]. However, they used different kinds of cells (AtT20 corticotroph cells) and conditions (starvation)

contrary to our study. Actually, intracellular energy depletion with the resultant activation of AMPK directly stimulates the HPA axis at the pituitary level by increasing the expression of POMC gene. The activation of AMPK in high glucose (4.5 g/L) leaded to the suppression of POMC in our research (Fig. 16). Thus the glucose level or intracellular energy status could be a crucial switch of the AMPK-mediated POMC regulation. In other report, Guillod-Maximin et al addressed that adiponectin receptors were expressed in hypothalamus and colocalized with POMC neurons in rodents, and adiponectin could activate AMPK in the rat [54]. However, they did not show any direct relevance of POMC itself and the activation of AMPK by adiponectin. Furthermore, Qi et al showed that adiponectin suppressed glucose level significantly and reduced POMC expression in a dose-dependent manner although this is not statistically significant [55]. As above, this reduction of POMC under AMPK activation should be understood in terms of obesity or nutrient-sufficient status.

Given that LXRα regulates POMC gene expression in the pituitary [45], we confirmed LXRα ligand increased POMC expression by using the synthetic LXRα ligand T0901317 and GW3965 hydrochloride. As shown in Fig. 16, both LXRα ligands upregulated the expression of POMC. However, when treated with metformin, POMC proteins were reduced although two kinds of LXR agonists were treated. Therefore, even in the presence of LXR agonist, metformin can be sufficient to inhibit LXRα via phosphorylating its threonine residue (Fig. 16). Taken together, it seems that the activation of AMPK by metformin could play a crucial role in POMC reduction under high glucose environment as like in the diabetic condition.

Hypothalamic AMPK has been suggested to act as a key sensing mechanism, responding to hormones and nutrients in the regulation of energy homeostasis. However, the precise neuronal populations and cellular mechanisms involved are

unclear. AMPK plays a critical role as a sensor of cellular energy status in many organs including heart, adipose cell, liver, pancreatic beta cell, skeletal muscle, and brain [56]. When it comes to the role of hypothalamic AMPK in cellular energy regulation, it has long been studied that hypothalamic AMPK activation has been important as a regulator of energy homeostasis [57]. Appropriate counter-regulatory response is crucial for recovery from too low or high glucose level, and AMPK activation appears to mediate this function. In other words, AMPK acts differently according to its environmental glucose or other nutrients levels are high or low. Insulin-induced hypoglycaemia in rats increased AMPK phosphorylation and α2AMPK activity in the hypothalamus [58]. Recently, Claret et al found that hypothalamic AMPK plays a critical role in glucose sensing by using mice lacking AMPK in POMC and agouti-related protein-expressing neurons [59]. Also, they showed that the lack of AMPK in POMC neurons led mice to obesity because of their suppressed metabolic rate and increased feeding. However, the role of AMPK activation under hyperglycemic status has not been elucidated thoroughly. This point has a quite important meaning in terms of the role of AMPK activation by metformin in diabetic patients. Furthermore, as shown in Fig. 15, metformin-induced acute AMPK phosphorylation also in its higher concentration supports the idea that hypothalamic AMPK is important in that the fast antihyperglycemic effect of metformin. Thus our finding that the activation of AMPK by metformin with plenty or enough of glucose would suppress POMC expression might provide a novel insight to the molecular mechanism of anti-diabetic action of metformin.

The reduced cortisol levels suggested that the rapid antihyperglycemic effect of metformin is attributed to the hypothalamic-pituitary-adrenal (HPA) axis, which we examined through *in vitro* and *in vivo* studies. We found the reduction of glucose, cortisol and ACTH resulted from the diminished POMC expression following AMPK and LXRα phosphorylation in the pituitary. In summary, the

antidiabetic effect of metformin occurs via the AMPK/LXRα/POMC pathway. The AMPK activator metformin suppresses POMC and ACTH expression levels in rat pituitaries through inhibitory phosphorylation of LXRα (Fig. 20).

Conclusion

Metabolic diseases including obesity and diabetes are complex multifactorial diseases arising from the interplay between a wide range of variables, such as eating habits, physical activity, and genetic factors. Metabolomic approach is comprehensive in scope and can measure as many metabolites as possible from biological samples simultaneously, without bias. Therefore, these metabolomic studies have great potential and are seen as a useful tool for the study of obesity and diabetes to investigate systemic alterations in metabolism or mechanism of its therapeutic drugs. In this study, significantly different metabolome signatures were showed and altered metabolites were identified in adolescent obesity (Part I) and metformin administration (Part II) groups.

Most obesity-associated morbidities are rare in children but common in adults. However, adolescent obesity is associated with adult obesity and impacts morbidities such as cardiovascular disease in adulthood. Therefore, investigating biomarkers for adolescent obesity has become crucial. In adolescent obesity biomarker study (Part I), multivariate statistical analysis showed clear discrimination between the untargeted metabolomes of nonobese and obese groups. Seven endogenous metabolites were distinguished in the obese group, and inflammation-related metabolite markers showed strong predictive power for group classification. From targeted metabolomics, 45 metabolites mostly related to inflammation were significantly different in the obese group. Our results showed that the increase of inflammation-related metabolites is a crucial metabolomic signature of obesity compared with normal weight in adolescents and that these metabolites may be useful for predicting cardiovascular risk. Furthermore, the metabolomic differences observed in this study suggested that adolescent obesity induces impending insulin resistance, ammonia toxicity, and oxidative stress.

Metformin is frequently prescribed for type 2 diabetes, however, the underlying mechanism by which metformin regulates blood glucose levels and/or affects pituitary remains unknown. In our mechanism study of metformin (Part II), the fluctuation of the metabolite cortisol indicated that the neuroendocrine system was involved in the anti-diabetic effect of metformin. And we found that metformin induced AMPK/liver X receptor α (LXRα) phosphorylation, followed by pro-opiomelanocortin (POMC) suppression in rats. To our knowledge, this is the first study to elucidate the antidiabetic mechanism of metformin, which decreases ACTH and cortisol by activating AMPK. Therefore, these findings increase our understanding of metformin which is the most widely used agent for the treatment and prevention of diabetes and insulin resistance syndrome by suggesting a novel antihyperglycemic mechanism of the drug. Furthermore, this study could alter existing mechanism of action of metformin, if confirmed and extended in further study. Also, this study provides the fundamentals for drug discovery and development of antidiabetic treatments targeting cortisol reduction.

Taken together, these large-scale and simultaneous analyses of huge numbers of metabolites in urine demonstrated that inflammation-driven insulin resistance, ammonia toxicity, and oxidative stress may represent crucial metabolomic signatures in obese adolescents, and the anti-hyperglycemic effect of metformin is attributed to reduced POMC/adrenocorticotropic hormone (ACTH)/cortisol levels following AMPK/LXRα phosphorylation in the pituitaries.

References

1. Vinayavekhin N, Homan EA, Saghatelian A. Exploring disease through metabolomics. *ACS Chem Biol* 2010; **5:** 91-103.

2. Spratlin JL, Serkova NJ, Eckhardt SG. Clinical applications of metabolomics in oncology: a review. *Clin Cancer Res* 2009; **15:** 431-440.

3. Dumas ME, Barton RH, Toye A, et al. Metabolic profiling reveals a contribution of gut microbiota to fatty liver phenotype in insulin-resistant mice. *Proc Natl Acad Sci U S A* 2006; **103:** 12511-12516.

4. Lee MS, Jung BH, Chung BC, et al. Metabolomics study with gas chromatography-mass spectrometry for predicting valproic acid-induced hepatotoxicity and discovery of novel biomarkers in rat urine. *Int J Toxicol* 2009; **28:** 392-404.

5. Zhang Y, Zhao J, Chu Z, Zhou J. Increasing prevalence of childhood overweight and obesity in a coastal province in China. *Pediatr Obes* 2015.

6. Biro FM, Wien M. Childhood obesity and adult morbidities. *Am J Clin Nutr* 2010; **91:** 1499S-1505S.

7. Lloyd LJ, Langley-Evans SC, McMullen S. Childhood obesity and adult cardiovascular disease risk: a systematic review. *Int J Obes (Lond)* 2010; **34:** 18-28.

8. Group, U. P. D. S. U. Effect of intensive blood-glucose control with metformin on complications in overweight patients with type 2 diabetes (UKPDS 34). *Lancet* **352**, 854-865 (1998).

9. Abbasi, F. *et al.* Effect of metformin treatment on multiple cardiovascular disease risk factors in patients with type 2 diabetes mellitus. *Metabolism* **53**, 159-164 (2004).

10. Phung, O. J., Scholle, J. M., Talwar, M. & Coleman, C. I. Effect of noninsulin antidiabetic drugs added to metformin therapy on glycemic control,

weight gain, and hypoglycemia in type 2 diabetes. *JAMA* **303**, 1410-1418, doi:10.1001/jama.2010.405 (2010).

11. Tahrani, A. A., Bailey, C. J., Del Prato, S. & Barnett, A. H. Management of type 2 diabetes: new and future developments in treatment. *Lancet* **378**, 182-197, doi:10.1016/S0140-6736(11)60207-9 (2011).

12. Moreno-Navarrete JM, O. F., Rodríguez-Hermosa JI, Sabater M, Pardo G, Ricart W, Fernández-Real JM. OCT1 Expression in adipocytes could contribute to increased metformin action in obese subjects. *Diabetes* **60**, 168-176 (2011).

13. Tosca, L. *et al.* Metformin decreases GnRH- and activin-induced gonadotropin secretion in rat pituitary cells: potential involvement of adenosine 5' monophosphate-activated protein kinase (PRKA). *Biol Reprod* **84**, 351-362, doi:10.1095/biolreprod.110.087023 (2011).

14. Zhou, G. *et al.* Role of AMP-activated protein kinase in mechanism of metformin action. *J Clin Invest* **108**, 1167-1174, doi:10.1172/JCI13505 (2001).

15. Labuzek, K. *et al.* Quantification of metformin by the HPLC method in brain regions, cerebrospinal fluid and plasma of rats treated with lipopolysaccharide. *Pharmacol Rep* **62**, 956-965 (2010).

16. Moon JS, Lee SY, Nam CM, et al. 2007 Korean National Growth Charts: review of developmental process and an outlook. *Kor J Pediatr* 2008; **51:** 1.

17. Rosenbaum PR, Rubin DB. The central role of the propensity score in observational studies for causal effects. *Biometrika* 1983; **70:** 41-55.

18. Römisch-Margl W, Prehn C, Bogumil R, Röhring C, Suhre K, Adamski J. Procedure for tissue sample preparation and metabolite extraction for high-throughput targeted metabolomics. *Metabolomics* 2011; **8:** 133-142.

19. Lord RS, Bralley JA. Clinical applications of urinary organic acids. Part 2. Dysbiosis markers. *Altern Med Rev* 2008; **13:** 292-306.

20. Calvani R, Miccheli A, Capuani G, et al. Gut microbiome-derived metabolites characterize a peculiar obese urinary metabotype. *Int J Obes (Lond)* 2010; **34:** 1095-1098.

21. Turnbaugh PJ, Ley RE, Mahowald MA, Magrini V, Mardis ER, Gordon JI. An obesity-associated gut microbiome with increased capacity for energy harvest. *Nature* 2006; **444:** 1027-1031.

22. Backhed F, Ding H, Wang T, et al. The gut microbiota as an environmental factor that regulates fat storage. *Proc Natl Acad Sci U S A* 2004; **101:** 15718-15723.

23. Altman R, Keenan AH, Newman JW, Rutledge JC. The postprandial effects of a moderately high-fat meal on lipid profiles and vascular inflammation in Alzheimer's disease patients: a pilot study. *J Gen Pract (Los Angel)* 2014; **2:** 186.

24. Feng B, Yao PM, Li Y, et al. The endoplasmic reticulum is the site of cholesterol-induced cytotoxicity in macrophages. *Nat Cell Biol* 2003; **5:** 781-792.

25. Mothe-Satney I, Filloux C, Amghar H, et al. Adipocytes secrete leukotrienes: contribution to obesity-associated inflammation and insulin resistance in mice. *Diabetes* 2012; **61:** 2311-2319.

26. Hotamisligil GS. Inflammation and metabolic disorders. *Nature* 2006; **444:** 860-867.

27. Koves TR, Ussher JR, Noland RC, et al. Mitochondrial overload and incomplete fatty acid oxidation contribute to skeletal muscle insulin resistance. *Cell Metab* 2008; **7:** 45-56.

28. Wallace M, Morris C, O'Grada CM, et al. Relationship between the lipidome, inflammatory markers and insulin resistance. *Mol Biosyst* 2014; **10:** 1586-1595.

29. Holland WL, Summers SA. Sphingolipids, insulin resistance, and metabolic disease: new insights from in vivo manipulation of sphingolipid metabolism. *Endocr Rev* 2008; **29:** 381-402.

30. Van Slyke DD, Phillips RA, Hamilton PB, Archibald RM, Futcher PH, Hiller A. Glutamine as source material of urinary ammonia. *J Biol Chem* 1943; **150:** 481-482.

31. Cooper AJ, Plum F. Biochemistry and physiology of brain ammonia. *Physiol Rev* 1987; **67:** 440-519.

32. Felipo V, Butterworth RF. Neurobiology of ammonia. *Prog Neurobiol* 2002; **67:** 259-279.

33. Alemany M. The problem of nitrogen disposal in the obese. *Nutr Res Rev* 2012; **25:** 18-28.

34. Babizhayev MA, Seguin MC, Gueyne J, Evstigneeva RP, Ageyeva EA, Zheltukhina GA. L-Carnosine (beta-alanyl-L-histidine) and carcinine (beta-alanylhistamine) act as natural antioxidants with hydroxyl-radical-scavenging and lipid-peroxidase activities. *Biochem J* 1994; **304:** 509-516.

35. Rauen U, Klempt S, de Groot H. Histidine-induced injury to cultured liver cells, effects of histidine derivatives and of iron chelators. *Cell Mol Life Sci* 2007; **64:** 192-205.

36. Lucotti P, Setola E, Monti LD, et al. Beneficial effects of a long-term oral L-arginine treatment added to a hypocaloric diet and exercise training program in obese, insulin-resistant type 2 diabetic patients. *Am J Physiol Endocrinol Metab* 2006; **291:** E906-912.

37. Mohanty P, Hamouda W, Garg R, Aljada A, Ghanim H, Dandona P. Glucose challenge stimulates reactive oxygen species (ROS) generation by leucocytes. *J Clin Endocrinol Metab* 2000; **85:** 2970-2973.

38. Zou, M. H. *et al.* Activation of the AMP-activated protein kinase by the anti-diabetic drug metformin in vivo. Role of mitochondrial reactive nitrogen species. *The Journal of biological chemistry* **279**, 43940-43951, doi:10.1074/jbc.M404421200 (2004).

39. Bergheim, I. *et al.* Metformin prevents alcohol-induced liver injury in the mouse: Critical role of plasminogen activator inhibitor-1. *Gastroenterology* **130**, 2099-2112, doi:10.1053/j.gastro.2006.03.020 (2006).

40. Buzzai, M. *et al.* Systemic treatment with the antidiabetic drug metformin selectively impairs p53-deficient tumor cell growth. *Cancer Res* **67**, 6745-6752, doi:10.1158/0008-5472.CAN-06-4447 (2007).

41. Meneton, P., Ichikawa, I., Inagami, T. & Schnermann, J. Renal physiology of the mouse. *Am J Physiol Renal Physiol* **278**, F339-351 (2000).

42. Khani, S. & Tayek, J. A. Cortisol increases gluconeogenesis in humans: its role in the metabolic syndrome. *Clin Sci (Lond)* **101**, 739-747 (2001).

43. Roy M, C. B., Roy A. Hypothalamic-pituitary-adrenal axis dysregulation among diabetic outpatients. *Psychiatry research* **31**, 31-37 (1990).

44. Vermes, I., Steinmetz, E., Schoorl, J., van der Veen, E. A. & Tilders, F. J. Increased plasma levels of immunoreactive beta-endorphin and corticotropin in non-insulin-dependent diabetes. *Lancet* **2**, 725-726 (1985).

45. Matsumoto, S. *et al.* Liver X receptor-alpha regulates proopiomelanocortin (POMC) gene transcription in the pituitary. *Mol Endocrinol* **23**, 47-60, doi:10.1210/me.2007-0533 (2009).

46. Hwahng, S. H., Ki, S. H., Bae, E. J., Kim, H. E. & Kim, S. G. Role of adenosine monophosphate-activated protein kinase-p70 ribosomal S6 kinase-1 pathway in repression of liver X receptor-alpha-dependent lipogenic gene induction and hepatic steatosis by a novel class of dithiolethiones. *Hepatology* **49**, 1913-1925, doi:10.1002/hep.22887 (2009).

47. Penniston, K. L. & Tanumihardjo, S. A. The acute and chronic toxic effects of vitamin A. *Am J Clin Nutr* **83**, 191-201 (2006).

48. Rolo, A. P., Oliveira, P. J., Moreno, A. J. & Palmeira, C. M. Bile acids affect liver mitochondrial bioenergetics: possible relevance for cholestasis therapy. *Toxicological sciences : an official journal of the Society of Toxicology* **57**, 177-185 (2000).

49. Woudenberg-Vrenken, T. E., Conde de la Rosa, L., Buist-Homan, M., Faber, K. N. & Moshage, H. Metformin protects rat hepatocytes against bile acid-induced apoptosis. *PLoS One* **8**, e71773, doi:10.1371/journal.pone.0071773 (2013).

50. SA, C. Betaine in human nutrition. *Am J Clin Nutr* **80**, 539-549 (2004).

51. Anedda, A., Rial, E. & Gonzalez-Barroso, M. M. Metformin induces oxidative stress in white adipocytes and raises uncoupling protein 2 levels. *The Journal of endocrinology* **199**, 33-40, doi:10.1677/JOE-08-0278 (2008).

52. Wile, D. J. & Toth, C. Association of metformin, elevated homocysteine, and methylmalonic acid levels and clinically worsened diabetic peripheral neuropathy. *Diabetes Care* **33**, 156-161, doi:10.2337/dc09-0606 (2010).

53. Iwasaki, Y. *et al.* Activation of AMP-activated protein kinase stimulates proopiomelanocortin gene transcription in AtT20 corticotroph cells. *Am J Physiol Endocrinol Metab* **292**, E1899-1905, doi:10.1152/ajpendo.00116.2006 (2007).

54. Guillod-Maximin, E. *et al.* Adiponectin receptors are expressed in hypothalamus and colocalized with proopiomelanocortin and neuropeptide Y in rodent arcuate neurons. *The Journal of endocrinology* **200**, 93-105, doi:10.1677/JOE-08-0348 (2009).

55. Qi, Y. *et al.* Adiponectin acts in the brain to decrease body weight. *Nature medicine* **10**, 524-529, doi:10.1038/nm1029 (2004).

56. Kahn, B. B., Alquier, T., Carling, D. & Hardie, D. G. AMP-activated protein kinase: ancient energy gauge provides clues to modern understanding of metabolism. *Cell Metab* **1**, 15-25, doi:10.1016/j.cmet.2004.12.003 (2005).

57. Ramamurthy, S. & Ronnett, G. V. Developing a head for energy sensing: AMP-activated protein kinase as a multifunctional metabolic sensor in the brain. *J Physiol-London* **574**, 85-93, doi:DOI 10.1113/jphysiol.2006.110122 (2006).

58. Han, S. M. *et al.* Hypothalamic AMP-activated protein kinase mediates counter-regulatory responses to hypoglycaemia in rats. *Diabetologia* **48**, 2170-2178, doi:10.1007/s00125-005-1913-1 (2005).

59. Claret, M. *et al.* AMPK is essential for energy homeostasis regulation and glucose sensing by POMC and AgRP neurons. *J Clin Invest* **117**, 2325-2336, doi:10.1172/JCI31516 (2007).

국문 초록

조 금 선

서울대학교 대학원 의과학과

의과학 전공

대사체학은 질환의 중증도 평가와 진단 및 기전 연구를 위한 생체표지자 발굴에 있어서 매우 효율적인 방법이다. 이는 생체시료에 존재하는 다양한 대사체들을 대상으로 동시 분석 가능한 방법이며, 특히 비만 및 당뇨와 같은 대사질환 연구에서 유용할 수 있다. 본 연구자는 대사체 분석법을 이용하여 비만과 이의 합병증 관련 생체표지자 발굴 연구와 당뇨약의 치료기전 연구를 수행하였다.

정상체중(93 명)과 비만(91 명) 청소년들을 대상으로 한 비만 및 합병증 관련 생체표지자 발굴 연구에서 high-performance liquid chromatography (LC)-quadrupole time-of-flight mass spectrometry (MS)와 LC- and flow injection analysis-MS/MS systems 각각을 기반으로 한 언타겟티드(untargeted) 및 타겟티드(targeted) 대사체 분석법을 통해 두 그룹 간에 유의한 차이를 보이는 대사체들을 프로파일링 하였다. 또한 당뇨약의 치료기전 연구에서는 14 명의 건강한 남성 지원자들을 대상으로 1000 mg 의 메포민(metformin)을 단 회 복용하게 한 후, 복용

전과 후의 아침 첫 소변을 이용한 대사체 프로파일링과 세포 및 동물을 이용한 분자생물학 실험을 하였다.

청소년비만의 생체표지자 발굴 연구에서 정상체중과 비만 청소년 대사체 그룹의 차이가 뚜렷함을 확인했다. 이는 정상체중과 비만 청소년에 대한 예측력이 높았던 염증 관련 대사체들을 포함한 7 개의 대사체로 인한 것이었으며, 다른 염증 관련 대사체들을 추가 분석한 결과에서도 45 개의 대사체들이 정상체중과 비만 청소년 그룹에서 유의한 차이를 보였다. 메포민을 이용한 당뇨약 치료기전에 대한 대사체 연구에서는 코티졸(cortisol)을 통한 신경내분비계의 변화가 주요한 결과였고, 이는 세포 및 동물 실험 결과 AMPK 및 liver X receptor α (LXRα)의 인산화(phosphorylation)와 pro-opiomelanocortin (POMC) 발현 감소를 통한 것임을 알 수 있었다.

결론적으로 본 연구자는 대사체학을 통하여 청소년 비만과 같은 대사질환과 메포민과 같은 대사질환 치료제를 대상으로 한 연구를 수행하여 관련 생체표지자의 발굴과 기전에 관한 연구 결과를 얻을 수 있었다. 요약하면, 정상체중과 비교하여 비만한 청소년에서는 염증반응과 관련한 인슐린 저항성, 암모니아 독성, 산화 스트레스 관련 대사체들의 발현이 증가되어 있음을 알 수 있었고, 메포민의 당뇨병 치료기전 연구에서는 뇌하수체에서의 AMPK 및 LXRα의 인산화에 의한 POMC/adrenocorticotropic hormone (ACTH)/cortisol 의 발현 감소가 메포민의 혈당강하 효과를 유도함을 알 수 있었고, 이들 결과는 대사체학이 대사질환 및 이의 합병증에 대한 발병 및 치료 기전 연구에서 중요하게 활용될 수 있을 것임을 암시한다.

주요어: 대사체학, 생체표지자, 청소년 비만, 당뇨병, 메포민

학번: 2012-31163